TECHNISCHE UNIVERSITÄT WIEN
Vienna | Austria

MEDIZINISCHE UNIVERSITÄT WIEN

Diplomarbeit

High-field Magnetic Resonance-based visualization of new polymer and resin materials for tissue mimicking phantoms

ausgeführt zum Zwecke der Erlangung des akademischen Grades eines

Diplom-Ingenieurs (Dipl.-Ing.)

eingereicht an der TU Wien, im Rahmen des Studiums Master Biomedical Engineering, von

Paul Péry,

Mat.Nr.: 12126320

unter der Leitung von

Ao.Univ.Prof. Dipl.-Phys. Dr. Andreas Berg
Center for Medical Physics and Biomedical Engineering, MUW

Ao.Univ.Prof. Dipl.-Ing. Dr.techn. Martin Gröschl
E134-01 - Research Unit of Applied and Computational Physics, TUW

Wien, Juni 2023

Ich habe zur Kenntnis genommen, dass ich zur Drucklegung meiner Arbeit unter der Bezeichnung

DIPLOMARBEIT

nur mit Bewilligung der Prüfungskommission berechtigt bin.

Ich erkläre an Eides statt, dass die vorliegende Arbeit nach den anerkannten Grundsätzen für wissenschaftliche Abhandlungen von mir selbstständig erstellt wurde. Alle verwendeten Hilfsmittel, insbesondere die zugrunde gelegte Literatur, sind in dieser Arbeit genannt und aufgelistet. Die aus den Quellen wörtlich entnommenen Stellen, sind als solche kenntlich gemacht.

Das Thema dieser Arbeit wurde von mir bisher weder im In- noch Ausland einer Beurteilerin/einem Beurteiler zur Begutachtung in irgendeiner Form als Prüfungsarbeit vorgelegt. Diese Arbeit stimmt mit der von den Begutachterinnen/Begutachtern beurteilten Arbeit überein.

Ich nehme zur Kenntnis, dass die vorgelegte Arbeit mit geeigneten und dem derzeitigen Stand der Technik entsprechenden Mitteln (Plagiat-Erkennungssoftware) elektronisch-technisch überprüft wird. Dies stellt einerseits sicher, dass bei der Erstellung der vorgelegten Arbeit die hohen Qualitätsvorgaben im Rahmen der geltenden Regeln zur Sicherung guter wissenschaftlicher Praxis „Code of Conduct“ an der TU Wien eingehalten wurden. Zum anderen werden durch einen Abgleich mit anderen studentischen Abschlussarbeiten Verletzungen meines persönlichen Urheberrechts vermieden.

Stadt und Datum	*Unterschrift*

Acknowledgement

At this point, I would like to thank everyone who supported and motivated me while performing and writing this master thesis.

Firstly, my supervisor from the Medical University of Vienna, Ao.Univ.-Prof. Dipl.-Phys. Dr. Andreas Berg, who introduced me to the subject, practically trained me to the operation of a 3T human MR scanner and to the post-processing of MR data. He taught me with great precision the physical principles of MRI and its direct impact on the implementation of MR-pulse-sequences. He was always available to discuss the results, and gave me the opportunity to present them during oral presentations at the Medical University of Vienna. He also offered precious advice for the correction and improvement of my master thesis. I would like to thank you very much for your support and your share of deep knowledge during my master thesis.

I would also like to thank the team from the Center for Medical Physics and Biomedical Engineering taking part in this project of MR-visible materials for all the constructive exchange we had, always seeking for improvements: Priv. Doz. Dipl.-Ing. Ivo Rausch, leader of the project, and Markus Ortner for manufacturing the samples with talent.

The support of Dipl.-Ing. Michael Woletz for the implementation of the MATLAB routines and Dr.med.univ. Marcos Wolf for sharing knowledge on the VFA sequence and the usage of qMRLab is very appreciated.

I would also like to thank my supervisor from TU Wien, Ao.Univ.Prof. Dipl.-Ing. Dr.techn. Martin Gröschl for supervising the work for the TU Wien.

The research within this master thesis was supported by:

- AWS project P2372591, “MR visible polymer for medical imaging applications”
- Hochschuljubiläumsfonds der Stadt Wien; A. Berg Magnetresonanz Breitlinien Bildgebung; H-247/2001
- Medical University of Vienna, CMPBME, Intramural financial support (A. Berg)

Finally, I want to thank my family and friends. They were always there for support and motivation.

Kurzfassung

Polymer- oder Harzmaterialien werden in der Magnetresonanz-Tomographie (MRT) häufig verwendet. Sie sind Hauptbestandteile von Phantombehältern für die Qualitätskontrolle (QC) in der quantitativen MRT und von Gewebe-simulierenden Phantomen für Ausbildungszwecke. Die Anwendungen können auch auf die MR-geführte Strahlentherapie (Fixierungsvorrichtungen zur Vermeidung von Bewegungen) und die Nuklearmedizin (Abschwächungskorrekturen für PET-MR) ausgedehnt werden. Feste Polymer-Materialien können jedoch aufgrund des sehr schnellen Signalzerfalls (Relaxation) in der Regel nicht mit MRT sichtbar gemacht werden. Ein Team der Medizinischen Universität Wien hat ein neues Verfahren zur Herstellung von MR-sichtbaren festen Polymeren entwickelt und patentiert. Die Technik basiert auf der Einlagerung von Mikropartikeln, die durch die Absorption einer protonenreichen Flüssigkeit als MR-scihtbares Additiv dienen, mit der Möglichkeit zur Einstelung einer breiten Palette von MR-Kontrast-Kenngrößen.

Diese Master Thesis ist die erste systematische QC-Untersuchung dieser neu hergestellten Materialien mit Standard-MRT. Visualisierende und quantifizierende Messungen wurden am Hochfeld-MR-Zentrum der Medizinischen Universität Wien durchgeführt. Die vollständige Qualitätskontrolle der quantitativen MRT-Parameter T2/T2*, T1 und Homogenität der Proben wurde auf einem 3T Hochfeld-MR Tomographen durchgeführt. Durch die richtige Auswahl der Art der Flüssigkeitszusätze (Öle, Wasser) können wir Originalmaterialien mit unterschiedlichen T1- und T2-Werten erzeugen. Die Untersuchung des Einflusses von Flüssigkeitszusatz und Konzentration auf T1 und T2 ermöglicht eine direkte Modifizierung und Verbesserung des Herstellungsprozesses. Um eine präzise, wiederholbare und schnelle T1-Bildgebung (T1-map) zu erreichen, wurden drei Sequenzen verglichen: die "Inversion Recovery" (IR), "Variable Flip Angle" (VFA und die "Progressive Saturation Recovery" (PSR) Sequenz. Die Nachbearbeitung der Daten erfolgt schließlich durch eine Multi-Schicht Analyse mit Routinen, die nicht direkt in der MR-Tomographen Software implementiert sind: Entfernung der ersten Echos zur Vermeidung von MR-Artefakten durch stimulierte Echos, 3-Parameter-Regressionsanalyse zur genaueren T1-Bestimmung, sowie der Anzeige der Regressionskurven zusammen mit den Daten von einzelnen Voxeln.

Die im Rahmen dieser Masterarbeit durchgeführten Arbeiten zeigen erstmals, dass durch die Auswahl verschiedener Arten von Zusätzen homogene Polymer Proben mit einem grösseren Bereich von T1-Werten zwischen ca. 200 und 2000 ms und von T2-Werten

zwischen ca. 100 und 600 ms hergestellt werden können. Die Proben lassen sich nachweislich auch erfolgreich im 3D-Druckverfahren herstellen, wobei ihre MR-Sichtbarkeit erhalten bleibt. Diese Ergebnisse unterstreichen die Perspektiven des Herstellungsverfahren für die Entwicklung gewebespezifischer Phantome, von Qualitätskontrollinstrumenten für MRT-Scanner, von Fixierungsvorrichtungen für die Strahlenplanung in der Strahlentherapie sowie für Abschwächungskorrekturen von MR-PET-Scannern in der Nuklearmedizin.

Abstract

Polymer or resin materials are widely used with reference to Magnetic Resonance Imaging (MRI). They are major constituents of phantom containers for Quality Control (QC) in quantitative MRI, and of tissue mimicking phantoms for educational purposes. Applications can also be extended to MR-guided radiation therapy (fixation devices for avoiding motion), and nuclear medicine (attenuation corrections for PET-MR). However, solid polymer materials usually cannot be visualized with MRI due to the very short signal relaxation. A new material manufacturing process for producing MR-visible solid polymers has been developed and patented by a team from the Medical University of Vienna. The technique is based on the embedding of micro-particles, which serve as an MR visible additive by absorbing a proton-rich fluid, with the potential of adjusting a wide range of MR contrast parameters.

This thesis is the first systematic QC investigation of these newly manufactured materials with standard MRI. Visualizing and quantifying measurements were conducted at the High-Field-MR-Centre of the Medical University of Vienna. Full quality control on quantitative MRI parameter mapping T2/T2*, T1 and homogeneity of the samples were performed on a high-field 3T scanner. By properly selecting the type of liquid add-ons (oils, water), we achieve to create original materials with varying T1 and T2-values. The study of the impact of liquid add-on and concentration on T1, T2 allows direct modification and improvement of the manufacturing process. Moreover, to reach precise, repeatable and quick T1 mapping, three sequences are compared: Inversion Recovery (IR), Variable Flip Angle (VFA) and Progressive Saturation Recovery (PSR). The data post-processing is finally realized by multi-slice analysis, with routines not directly implemented in the MR-scanner software: removal of first echoes for avoiding stimulated echo MR-artefacts, 3-parameter regression analysis for more accurate T1 determination as well as the display of the regression curves together with the measurement data of single voxels.

For the first time, the work performed within this master thesis demonstrates that by adjusting the types of add-ons, homogeneous polymer samples can be produced with a wide range of T1 values, between about 200 ms and 2000ms, and T2 values between 100 ms and 600 ms. The samples are also proved to be successfully 3D-printed, while keeping their MR-visibility. These results indicate the perspectives of the manufacturing method

for the development of tissue specific phantoms, of quality control tools for MRI scanners, of fixation devices in radiation planning for radiation therapy, as well as for attenuation corrections of MR-PET scanners in nuclear medicine.

Contents

List of Figures

[1].

[2].

Acronyms

2DFT 2-Dimensional Fourier-transformation.

AWS Austrian Wirtschaft Service.

BPP Bloembergen-Purcell-Pound.

CAD Computer Aided Design.
CMPBE Center for Medical Physics and Biomedical Engineering.
CPMG Carr-Purcell-Meiboom-Gill.

DLP Digital Light Processing.

FID Free Induction Decay.
FOV field of view.

GE Gradient Echo.

IR Inversion Recovery.

MRI Magnetic Resonance Imaging.

PLA polylactic acid.
PMMA Polymethyl Methacrylate.
PSR Progressive Saturation Recovery.
PVA Poly(vinyl alcohol).

QA Quality Assurance.
QC Quality Control.

RF Radio-Frequency.
ROI Region Of Interest.

SNR Signal-to-Noise-Ratio.

TE Echo time.

TI Inversion time.

TR Repetition time.

TSE Turbo Spin Echo.

UTE Ultra-short Time Encoding.

VFA Variable Flip Angle.

1 Introduction

Polymeric materials are substances which are composed of molecules characterized by multiple repetitions of constitutive units. They are mainly chosen in the medical field because of their bio-compatibility and sufficient mechanical properties (hardness, strength, toughness, resistance to fracture). Polymer materials used in clinical routine cover a very wide range of applications as implants, fixations or quality control devices of imaging modalities. Phantoms mimicking patient anatomy are of significant interest to calibrate and optimize imaging devices. However standard clinical Magnetic Resonance Imaging (MRI) is not capable to detect signals from large molecules like proteins, collagen fibers and of course polymers. The difficulty to perceive signal from polymers using MRI is due to their very quick MR-signal decay related to the limitation in the mobility of the large molecules [Bloembergen et al., 1948].

Two main values characterize the MR signal and are responsible for contrast in the image: T1 and T2. These relaxation times are specific for each type of medium. T1 and T2 are related and determined mainly by the mobility of the molecules:

- Liquids like water for instance will have very high T2 in comparison to solids which will have short T2. This dependence of T2 on mobility might result in hyperintense areas for tissue compartments with high liquid contribution (e.g. lymph area) and hypointense or even no signal for tissue or implant material with high concentration of immobile long molecules (e.g. tendons or polymers).
- Molecules not moving, vibrating or tumbling, which corresponds to a more solid type of material with high molecular mass will exhibit a short T2. Contrariwise, mobile molecules will have a long T2 [Bloembergen et al., 1948].

In their investigations, [Talalwa et al., 2019] reported on "3D printable rubber-elastomeric polymers" producing MR signal. However, these materials are not rigid but of spongeous type and therefore very soft, not corresponding to the qualification of a rigid material. A

solid resin has been used by [Rai et al., 2020] in order to build 3D printed MRI-phantoms. It is the "High Temperature material (RGD525)" from the American manufacturer Stratasys (Minnesota/USA), which composition is privately protected in a trade secret. But this material delivers low T1 = 150 ± 6.7ms and T2 = 56.1 ± 3.9ms, limiting its potential applications.For these reasons there are nowadays no imaging phantoms made of rigid polymer resin only. Most of the phantoms are constructed of plastic filled with signal-producing liquids or gels. But these present several disadvantages like flow artefacts or degradation of the gels with time. As imaging phantoms are used for quality control and research in the field of MRI, their mechanical, physical and chemical stability are relevant. MRI visible resins would be of great interest to replace the present phantoms. Applications can be also extended: in the field of PET-MR, for example, MR-visible radio-frequency (rf) coil housings and fixation devices would avoid the necessity for additional CT for attenuation corrections.

These observations motivated a team from Center for Medical Physics and Biomedical Engineering (CMPBE), in cooperation with the High field MR-center of the Medical University of Vienna, to develop a manufacturing process to produce an MR visible resin. A light-curable resin composition is mixed with add-ons capable of producing an MRI signal. The material has been patented in the European Union [Rausch et al., 2022] and has gained a financial support from the Austrian Wirtschaft Service (AWS), for prototype development: "PRIZE", project nr. P2372591, "MR visible polymer for medical imaging applications", project managers: Ivo Rausch and Christiane Galhaup, cooperating partners: Ewald Unger and Andreas Berg.

The present master thesis is related to this project and aims at providing a systematic study for assessing the MRI signal properties of the delivered samples, by means of T1, T2 and T2* relaxation times and signal homogeneity. The practical work within this master thesis followed the subsequent secondary objectives:

1. Console operation on a clinically used High field 3T MR-scanner on reference samples delivered by the cooperating manufacturing group, for quantitative parameter mapping and high-resolution MRI.
2. Development of MATLAB routines, not directly implemented within the MR-scanner software, for: first echo-removal in T2 weighted image data sets, multi-slice T2 and T1 parameter mapping (fitting of differently weighted data sets).
3. Multi-slice evaluation of T1, T2 on the different samples.

4. Quantitative comparison of different MR-pulse-sequences and protocols for the measurement of T1 and T2.

In the following sections, first the physical principles of MRI are presented, as theoretical basis of this work. In order to define the framework of the study, both the characteristics of the manufactured resin and the choice of the MR sequences for quantitative T1 and T2 mapping are then explained. The MATLAB routines for T1 and T2 assessment are also described within the "Materials and Methods" section. Finally, the results of the MR measurements and the assessment of T1, T2 and T2* and homogeneity of the samples are reported. These are finally discussed and concrete applications are presented.

2 Theoretical Background

2.1 Magnetic resonance

Magnetic Resonance Imaging (MRI) is an non-invasive imaging technique based on the visualization of nuclear spin distributions mainly in biological tissue but also in other materials. Although other nuclei can be detected, hydrogen (^1H) is the most used nucleus. In principle, this is due to its high natural abundance in biological systems, which implies a strong MR signal of the sample. In the following parts exclusively ^1H MR is considered.

2.1.1 Nuclear spin precession

Hydrogen nucleus consists of a proton which is a subatomic particle with a unique positive charge $e = +1,610^{-19}C$. It has electrical and magnetic properties.

Within a magnetic point of view, the proton is described as a dipole. It is a vector with a norm called the magnetic moment, μ. Major properties of magnetic dipoles are to respond to exterior magnetic fields and to generate their own magnetic field.

The proton has also quantum mechanical properties: It is quantified by an intrinsic angular momentum, called "nuclear spin" or "spin", with a value $I = \frac{1}{2}$.

Both the spin and the magnetic moment are linked according to the relation :

$$\mu = \gamma I \tag{2.1}$$

$\gamma = \frac{g_I \mu_N}{\hbar}$ is the gyromagnetic ratio, with g_N the characteristic nuclear g-factor and μ_N the nuclear magneton defined in analogy to the Bohr magneton. [Demtröder, 2016]

In comparison to other stable nuclei hydrogen has a high gyromagnetic ratio:
$\frac{\gamma}{2\pi}$ = 42,6 MHz/T [Reiser et al., 2007]

Subsequently the behavior of nuclear spins is described within a simple classical model with some add-ons introducing some quantum mechanical aspects (e.g discretized spin states in a magnetic field). The latter is applicable for a high number of nuclear spins with macroscopic magnetization, but the dynamics of a singular nuclear spin cannot be described within this model.

When no external magnetic field is applied, the behavior of protons is random and mainly due to thermal agitation. The orientation of the dipoles changes constantly because of molecular vibrations, rotations and collisions. The angular distribution is therefore statistically unordered and the magnetization vector is directed to different varying directions. In a Cartesian coordinate system the sum of the projection on the axis x, y, z of all these magnetic moments is null: M=0, with **M** the vectorial sum of the magnetic moments of all protons.

The exposure to a static external magnetic field B_0, applied in a unique direction (often the z-axis is taken as reference), results in an ordering effect of the random orientation of the magnetic moments. Following the laws of quantum mechanics the spins of the protons can have only two precise values and therefore projections along the z-axis [Reiser et al., 2007]:

- Spin "UP" : $m = +\frac{1}{2}$, orientation parallel to B_0 the outer magnetic field
- Spin "DOWN" : $m = -\frac{1}{2}$, orientation anti-parallel to B_0

In a classical model description, the magnetic moment of the proton experiences a torque due to the static magnetic field B_0. The result is a precession movement of the protons around the z-axis at a frequency called the Larmor frequency:

$$\omega_L = \gamma B_0 \tag{2.2}$$

On a microscopic scale the distribution of spins of hydrogen nuclei in a sample is following Boltzmann statistics in thermal equilibrium [Demtröder, 2016]:

$$\frac{N_{UP}}{N_{DOWN}} = e^{\frac{-2\mu_z B_0}{kT}} \tag{2.3}$$

with k the Boltzmann constant and T the temperature.

M has two components:

- Longitudinal magnetization M_z, the component along the z-axis.
- Transverse magnetization M_{xy}, projection to the xy-plane.

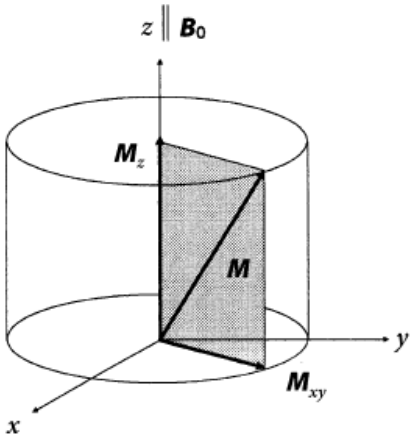

Figure 2.1: The vectorial sum of the moments of all protons **M** and projection to the xy-plane and the z-axis.[Reiser et al., 2007]

In a static magnetic field B_0, oriented along the z-axis, a minimal surplus of magnetic moments aligns parallel to B_0, as nuclei will strive for occupying the lowest energy level. This results in a small macroscopic magnetization in positive z-direction, which is essential for the detection of an MR signal. Only this small amount contributes to the total nuclear magnetization as the rest of them cancels each other out. On the xy-plane the precession is at the same speed for a perfectly homogeneous field, but might follow a different phase: the transverse magnetization $M_{xy} = 0$.

At this stage no signal can be yet detected.

2.1.2 Resonance

In order to detect a signal from the previous configuration an additional magnetic field B_1 is applied in the (x,y) plane. The latter is much smaller than B_0 but oscillating at the same Larmor frequency as the protons. This is done by generating electromagnetic waves (RF-pulses) using radio frequency coils.

During resonant excitation of the spin system, the rf-transmitter system transfers rf-energy from the rf-pulses originating from the rf-amplifier to the nuclear sin system. This results in a transition of the proton spin states from the lower energy level ("DOWN") to higher energy level ("UP"). As depicted on the scheme for Zeeman splitting in figure 2.2, the excess of protons in the level "DOWN" compared to the level "UP" is reduced. Consequently the longitudinal magnetization M_z decreases to zero.[Oystaeyen, 2018]

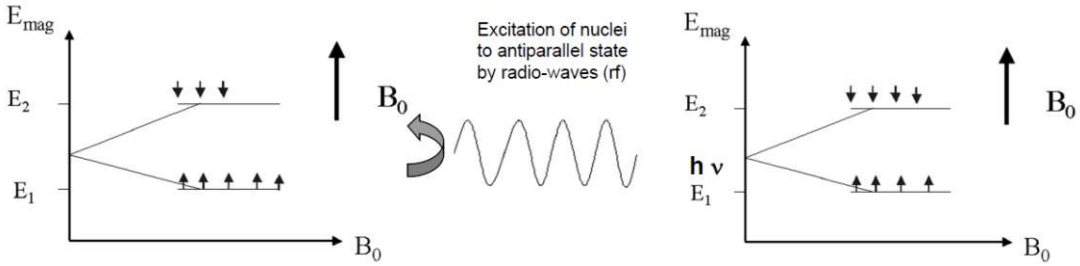

Figure 2.2: Scheme for Zeeman spliting with energy levels and spin orientation before (left) and after (right) rf-pulse excitation. E1 is the state of lower energy, while E2 is the state of higher energy[1]

The adjustments in timing, strength and length of rf-pulses allow for setting of the flip angle with reference to B0 direction and phase of the dynamics of the transverse magnetization [Czerny, 2022].

The relaxation process is characterised by two relaxation times called “spin-lattice” and “spin-spin relaxation”. The latter are material-dependent, resulting in different image contrast.

[1]Berg, A. (2021). Postgraduate University Course: "Medical Physics", lecture handouts: Magnetic Resonance 1; Medical University of Vienna, WS 2021/2022

2.2 Relaxation mechanisms and detection

During resonance the longitudinal and the transverse magnetization were linked through the relation $M^2 = M_z^2 + M_{xy}^2$. [Oystaeyen, 2018] After the excitation by a 90° rf-pulse, B_1 is turned off and the resonance stops. The system tends also to gradually return to its initial state. The longitudinal magnetization M_z, which reached zero, starts to grow again and gradually returns to its initial value M_0. The transverse magnetization M_{xy} starts to decrease and quickly returns to its initial value of zero.

2.2.1 T1 - Longitudinal relaxation

The longitudinal relaxation, also called "spin-lattice relaxation", characterizes the increasing longitudinal magnetization M_z back to the initial state. Energy is transferred to the molecular lattice of the sample.

This phenomenon is described mathematically by an increasing exponential to a final saturation value M0, with time constant T1, according to Bloch equations [Bloch, 1946]:

$$M = M_0 \cdot (1 - e^{-t/T1}) \tag{2.4}$$

"T1 is the longitudinal relaxation time. It gives the time required for the longitudinal magnetization after a 90° rf-pulse to reach 63% of its equilibrium value M_0" [Reiser et al., 2007] (Figure 2.3).

T1 is significant for image contrast as the recovery depends on the medium. Relaxation is indeed a complex phenomenon, which relies on multiple physical mechanisms:

- Dipole-dipole interactions,
- Chemical shift anisotropy,
- Molecular translation/flow/diffusion,
- Chemical exchange,
- Scalar (J-coupling),
- Electric-Quadrupole coupling. [Elster, 2023]

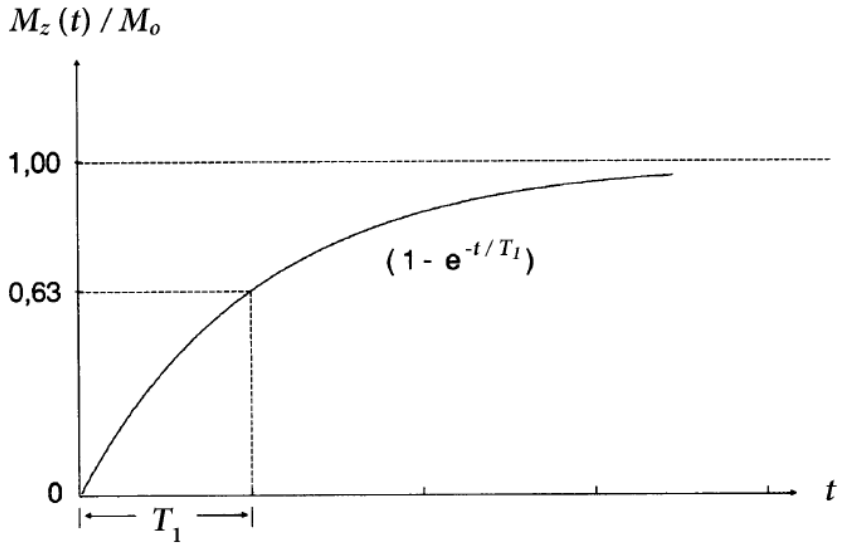

Figure 2.3: Longitudinal magnetization relaxation profile [Reiser et al., 2007]

For T1 contrast, the dipole-dipole interaction is playing a major role. Dipoles (proton, electron, nucleus) create indeed local electromagnetic fields, which interact through space. These dipolar interactions depend on:

1. the types of spins (proton-proton vs proton-electron),
2. their spatial relationship (distance, angle between them),
3. their relative motion.
4. the orientation of the magnetic moments.

They are mathematically described by the BPP-theory, named according to its authors Bloembergen, Purcell, and Pound. According to this model, the tumbling motion of molecules (rotation, translation or vibration) in the regime of the resonance frequency of the nucleus greatly affects the energy relaxation [Bloembergen et al., 1948].

In the case of homo-nuclear dipolar coupling and isotropic motion, the BPP-theory states:

$$\frac{1}{T1} \propto \frac{\tau_c}{(1+\omega^2\tau_c^2)} + \frac{4\tau_c}{(1+4\omega^2\tau_c^2)} \tag{2.5}$$

The longitudinal relaxation is dominated by molecular motion, which is characterized by the auto-correlation time τ_c. Usually solid types of tissue or materials are characterized by long τ_c, whereas short τ_c describes rather a fluid type.

This dependency of relaxation time on correlation time is plotted in figure 2.4. The longitudinal relaxation time exhibits a minimum when $\omega\tau_c = 1$. T1 begins to increase with ω and consequently B in the regimes $\omega\tau_c << 1$ and $\omega\tau_c >> 1$.

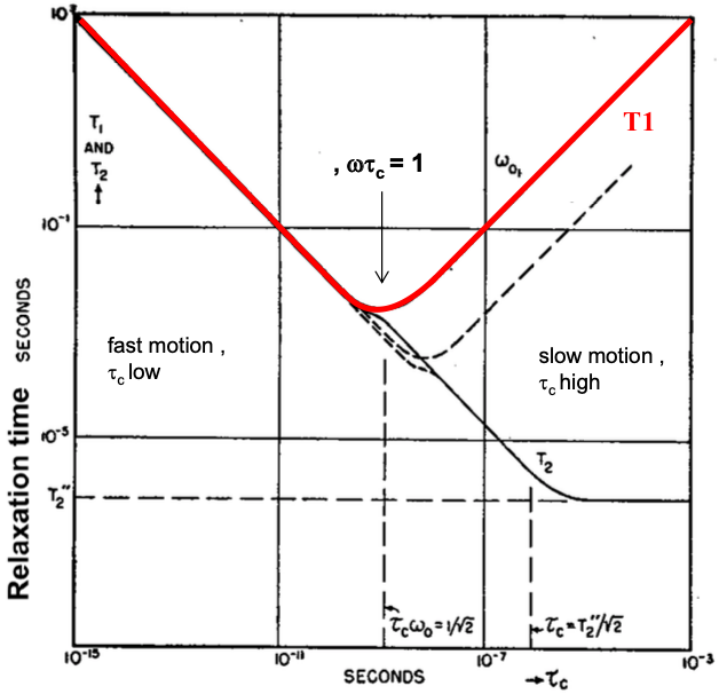

Figure 2.4: T1 as a function of τ_c according to the BPP-theory. [Bloembergen et al., 1948]

Contrast agents

T1 is mostly determined by the mobility of the molecules but changing the type of spins will also impact T1 contrast. It is the goal of contrast agents. The most common used contrast agents for MRI are iron ions (Fe3+), transition metals (Mn2+) and Lanthanides (Gd3+DTPA). These substances aim at enhancing the dipolar interactions. As the electronic magnetic moment is much stronger than the nuclear one, the electron-proton interaction is much more efficient than the proton-proton interaction. One contrast agent molecule can offer multiple magnetic interactions of nuclei with surrounding paramagnetic molecules. The direct consequence is the high sensitivity of T1 to such contrast agents."A contrast agent is very effective if a low concentration results in a strong change of the longitudinal relaxation rate 1/T1 in affected medium"[2].

[2]Berg, A. (2021). Postgraduate University Course: "Medical Physics", lecture handouts: Magnetic Resonance 1; Medical University of Vienna, WS 2021/2022

2.2.2 T2 - Transverse relaxation

The transverse relaxation, also called spin-spin relaxation, characterizes the decay of the transverse magnetization M_{xy} back to its initial state $M_{xy} = 0$.

This phenomenon is described mathematically by a decaying exponential with time constant T2, according to Bloch equations [Bloch, 1946]:

$$M = M_0 \cdot e^{-t/T2} \tag{2.6}$$

T2 is the transverse relaxation time. At $t = T2$, the transverse magnetization after a 90° pulse has fallen from its original magnitude to $\frac{M}{M_0} = e^{-1} = 37\%$. [Reiser et al., 2007]

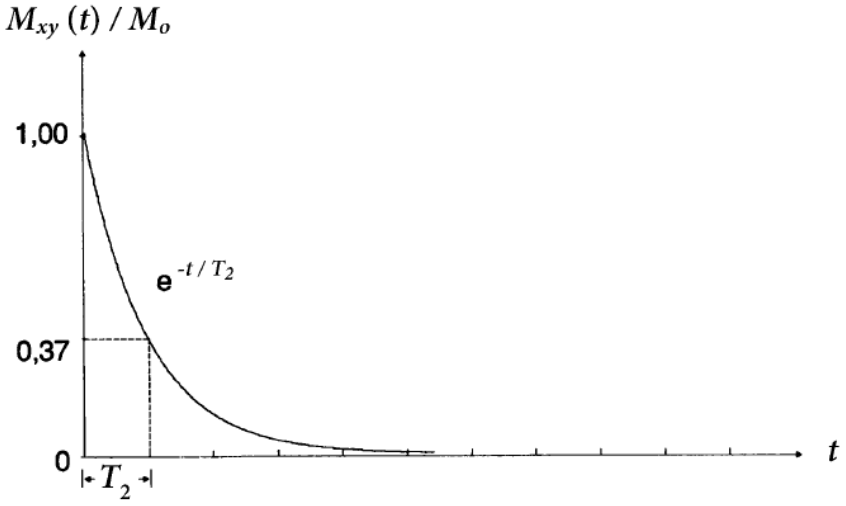

Figure 2.5: Transverse magnetization relaxation profile [Reiser et al., 2007]

The 90° rf-pulse has rotated the distribution of protons from the z-axis to the xy plane, but they are still ordered by the Boltzmann law. They are in "phase coherence". Dephasing of the components of the macroscopic transverse magnetization occurs when B1 is turned off. Small disturbances in the magnetic field implies different Larmor frequency and each components begin to turn at slightly different speeds. It results in the decrease of the transverse magnetization and therefore T2 relaxation.

This motion generates an induced current in antennas, therefore a signal can be acquired. This fundamental signal is called Free Induction Decay (FID).

As for T1, the relaxation process is described by the BPP-theory. Molecular motion is affecting the frequency spectrum of dipolar magnetic fields in the surrounding molecules of the observed nuclear spins.

In the regime $\omega\tau_c << 1$ the transverse relaxation rate $1/T2$ increases with correlation time τ_c:

$$1/T2 \propto \tau_c \tag{2.7}$$

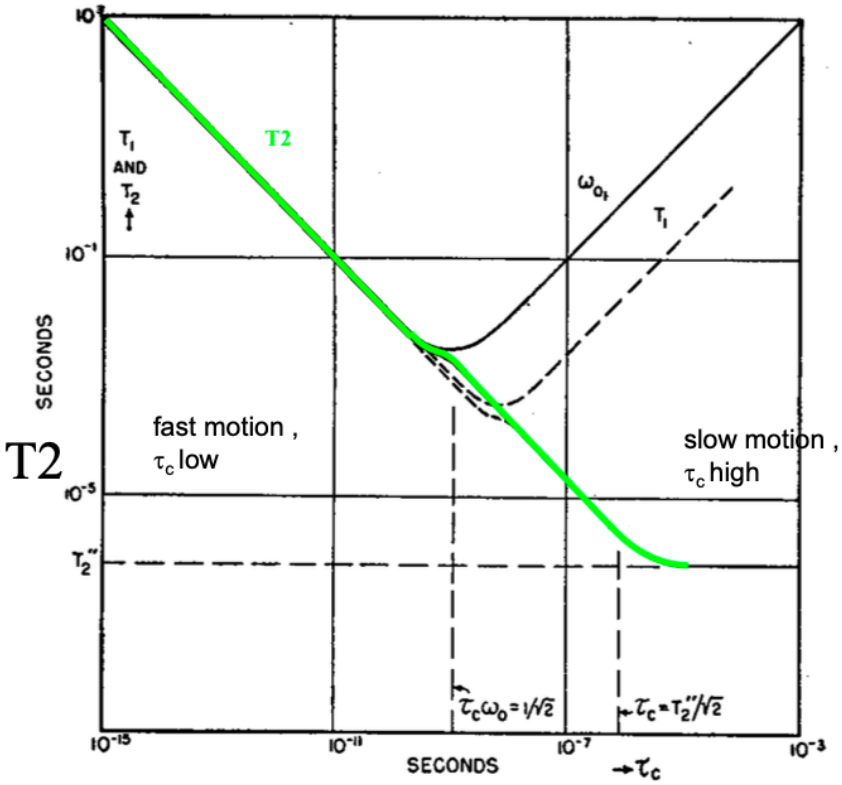

Figure 2.6: T2 in function of τ_c according to the BPP-theory. T2 exhibit a minimum when $\tau_c = \omega = 0$ (static condition). [Bloembergen et al., 1948]

The T2-time is dependent on the mobility of the molecules in tissue characterized by the mean time τ_c [Bloembergen et al., 1948]. Free mobile molecules have low correlation time τ_c, and therefore long T2. This corresponds to a fluid type of materials. On the contrary, molecules not moving, vibrating or tumbling or with higher molecular mass,

are characterized by long correlation times τ_c. Consequently, the latter, corresponding to more solid materials, exhibit short T2. "The effect of mobility on T2 and correspondingly line-width is called motional narrowing"[3].

2.2.3 T2* - Relaxation

Any disturbance to the magnetic field will accelerate the dephasing of the spins. It is of significant importance for imaging as the random movements of protons or the differences in the neighborhoods of protons will differ from one medium to another. However, disturbances come not only from the media but also from fluctuating local magnetic fields and spatial field inhomogeneities of the external field B_0, caused by technical imperfections. These phenomena induce an increasing of the dephasing and cause an additional relaxation rate $T2'$ which sums up with the intrinsic relaxation rate $1/T2$. Consequently it shortens even more the decay of the medium specific transverse relaxation time T2.

The effective transverse relaxation time is the combination of the effects of fluctuating local magnetic fields and spatial field inhomogeneities of the external field B_0. This time is noted $T2^*$:

$$\frac{1}{T2^*} = \frac{1}{T2'} + \frac{1}{T2} \tag{2.8}$$

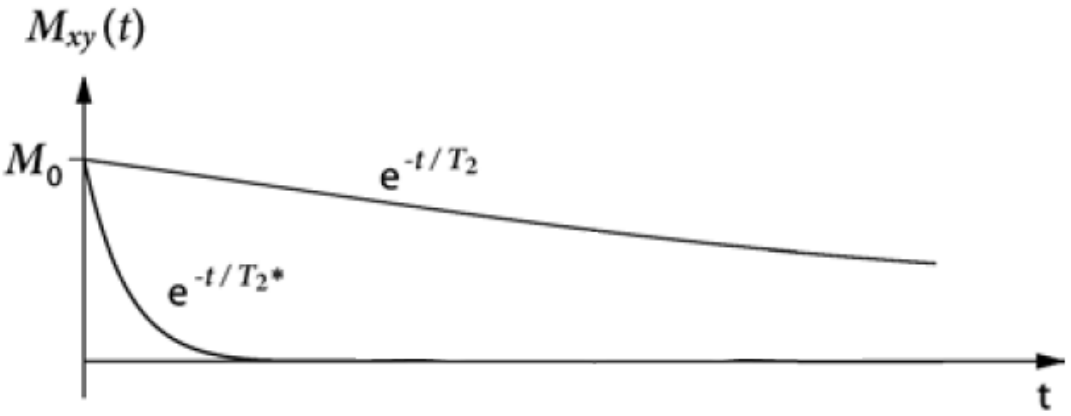

Figure 2.7: The FID decay is governed by $T2^*$ [Reiser et al., 2007]

T2* is very sensitive to magnetic susceptibility and inhomogeneities.

[3]Berg, A. (2021). Postgraduate University Course: "Medical Physics", lecture handouts: Magnetic Resonance 1; Medical University of Vienna, WS 2021/2022

2.3 MR Imaging

In this section the main principles for producing an image from the MR phenomenon are presented. The construction is developed following the spin-echo sequence (figure 2.9). More complex sequences rely on the same basis. Other sequences will be presented in the part "Material and Methods".

In order to create an image three elements are needed[4]:

1. Localisation
2. Signal
3. Contrast

As described in the previous parts, signal and contrast result from protons excitation in a static magnetic field B_0 and their relaxation with characteristic times T1, T2.

The localisation relies on the encoding of spatial information. The idea is to create space-depending inhomogeneities in the static magnetic field B_0 during the sequence. Tiny changes in the magnetic field imply an increase or decrease of the Larmor frequency of spins according to the equation 2.2. A specific Larmor frequency will be linked to a specific position (x, y, z) in space, allowing the spins to be differentiated. An image is then reconstructed.

In 2-Dimensional Fourier-transformation (2DFT) imaging, spatial encoding is a three step process, with :

1. Slice selection for determination of z
2. Frequency encoding for x
3. Phase encoding for y

First, a slice selective gradient $G_z = \frac{\Delta B}{\Delta z}$ imposes the resonance condition at a specific z-position. The RF-pulse is sent at the corresponding frequency :

$$\omega(z) = \gamma(B_0 + G_z z) \tag{2.9}$$

[4]Meyerspeer, M., Schmid, A. I. (2022) Basic Seminar: "Basics of MR Physics", lecture handouts; Medical University of Vienna WS2022

Only nuclear spins in this "slice" are excited.

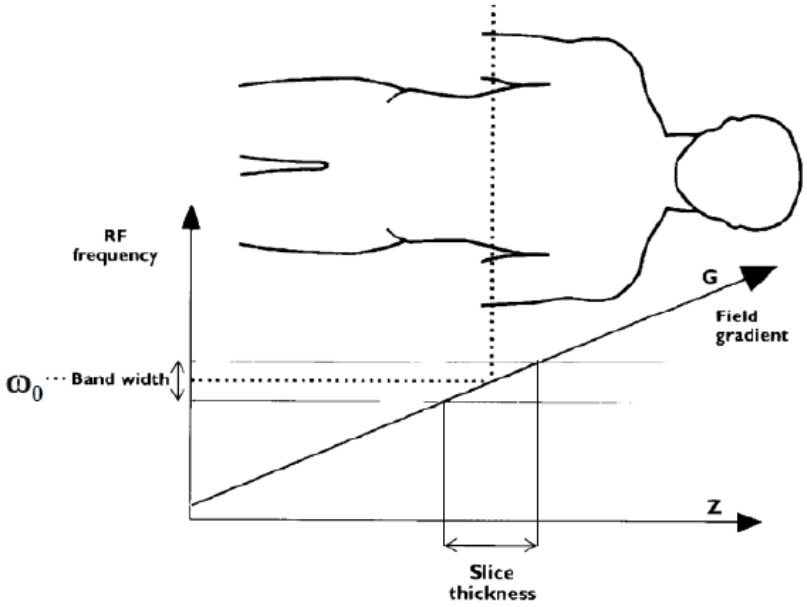

Figure 2.8: Field gradient for slice selection [Systems, 1990]

Even if the MR signal is complex, it can be decomposed by Fourier analysis into sinusoidal components : $I = I_0 \cos(\omega t + \phi)$. Once the slice is selected the three unknowns I_0, ω and ϕ encode respectively the gray level, the x position and the y position of the pixel.[Oystaeyen, 2018]

During spin precession a phase encoding gradient $G_y = \frac{\Delta B}{\Delta y}$ is applied during a time t. The latter introduces a phase shift to the spins, which depends on the y direction :

$$\phi(y) = \Delta\omega(y)\Delta t \tag{2.10}$$

Finally, during rf-detection a frequency encoding gradient $G_x = \frac{\Delta B}{\Delta x}$ is applied. The emitted radio-frequency ω is dependent on the magnetic field :

$$\omega(x) = \gamma(B_0 + G_x x) \tag{2.11}$$

Spins at a certain x-position, emit specific radio frequencies.

The sequence is repeated multiple times, each time with another phase encoding gradient G_y. The time between two sequences is called the repetition time TR.

The 2D-Fourier-transformation for frequency and phase-encoding signals finally offers a slice selective image. [Elster, 2023]

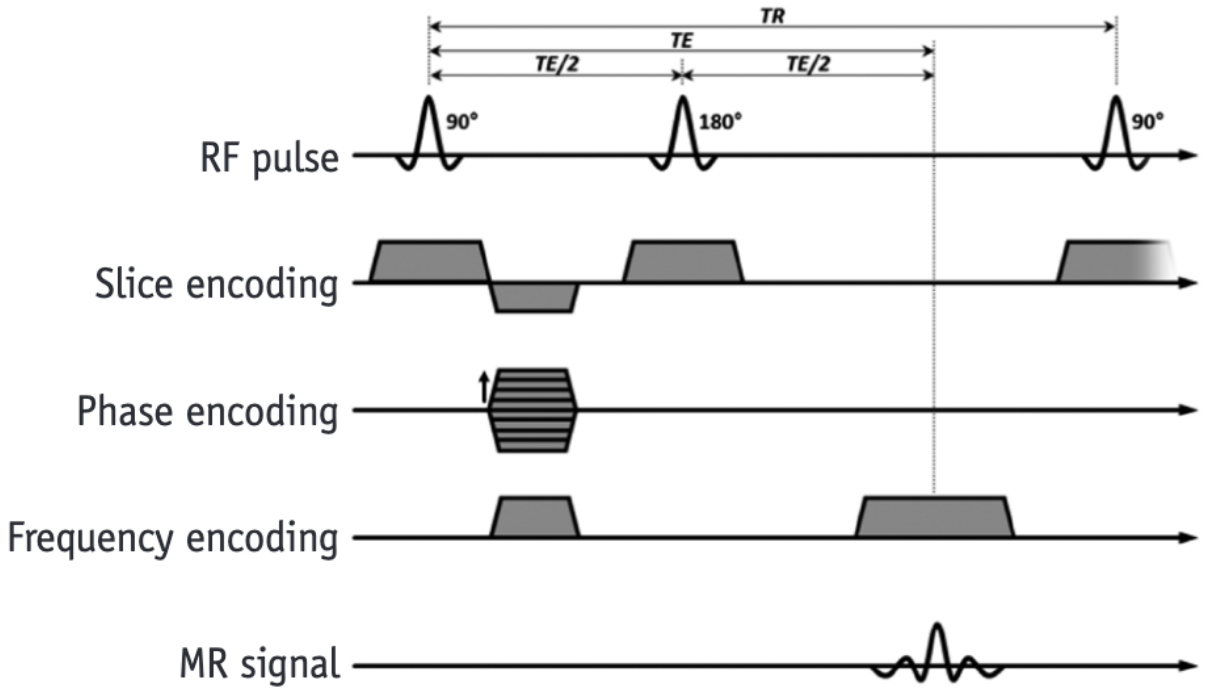

Figure 2.9: Scheme of the spin-echo sequence [Jo et al., 2019]

3 Materials and Methods

3.1 MRI phantoms :

3.1.1 State of the art

As seen in the previous parts, magnetic resonance imaging is a complex process. Many parameters play a significant role in the acquisition of the desired image. MRI scanners are therefore very sensitive and often need to be checked for quality control.

A phantom is a standard reference object which is used for mimicking tissues, but also for quality control of imaging modalities and for research. Its main function is to validate the accuracy and to assess the repeatability of the measurements performed by MRI. Performances of MR scanners evolve in time. Basic parameters such as signal-to-noise ratio (SNR), spatial resolution, homogeneity, T1 and T2 precision, and geometric distortion need therefore to be assessed regularly. The system can then be adjusted in order to ensure precise measurements.

Nowadays, even if the design depends on the application, most of the phantoms for MRI are build with the same structural elements:

- A frame composed of plastic materials like polymethyl methacrylate (PMMA)
- Compartments of different shape and forms filled with signal-producing liquids.

For example, the *Eurospin II Test System* has been an often used phantom in Europe (Figure 3.1). It is a set of cylindrical phantoms, each assessing different parameters : uniformity, slice profile, slice position, resolution, contrast. [Elster, 2023] The individual items are composed of chambers filled with an MR-visible liquid solution.

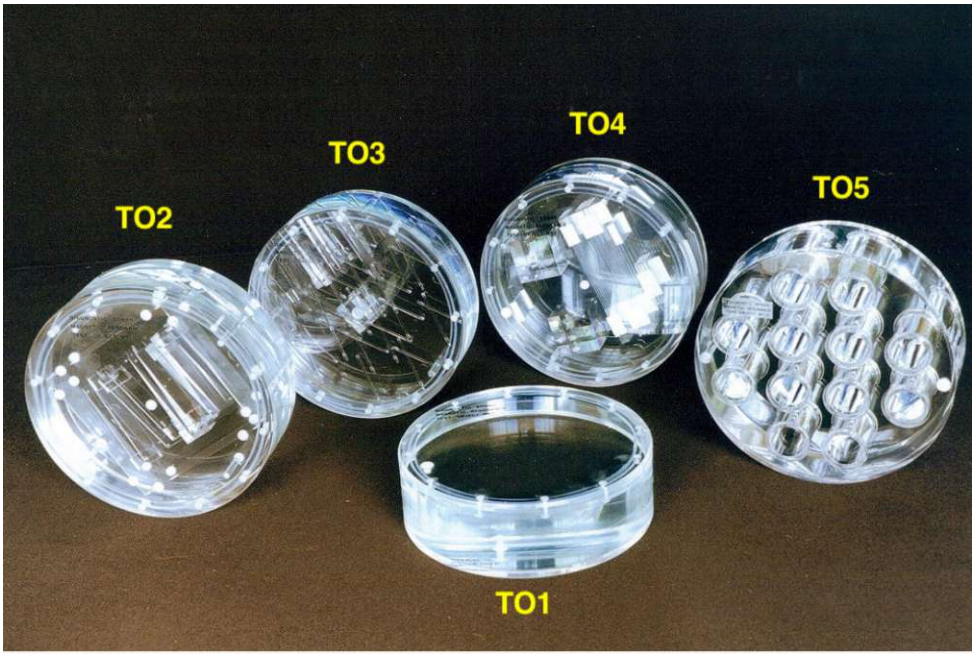

Figure 3.1: Set of the Eurospin II Test System [Elster, 2023]

These liquids are often based on doped water featuring the possibility for chemical changes due to diffusion and mobility of the molecule. Gels can also be used instead of liquids but there are several disadvantages with this approach in general.

Firstly, the long term stability of such phantom is not assured. Liquids and gels suffer in time from degradation, as fungi or bacteria may develop. Moreover, there is a significant problem due to the mobility of liquids inside the housing. The displacement of such liquid-filled phantoms results in turbulent flows, which might last even several minutes after positioning the phantom in the MR-scanner. Liquid-filled phantoms are also susceptible to contain air bubbles. The direct consequences are artefacts in MR-imaging, misleading the control assessments. In addition, the homogeneity of the phantom is a major requirement to ensure accurate standardization of MR protocols.

The development of an MR visible polymer must face these challenges. Members of the Center for Medical Physics and Biomedical Engineering developed a patented manufacturing concept for an MR-visible but solid resin material which is directly MR-visible [Rausch et al., 2022]. Within this master thesis the MR characteristics of the first higher number of batches of this material is investigated in a systematic way (AWS project P2372591, “MR visible polymer for medical imaging applications”).

3.1.2 3D printing materials

Figure 3.2: Ten samples of on site available polymers selected for MRI-visibility investigation.

In parallel to the analysis of the samples produced according to the European patent (EP3974903A1) at the CMPBE, investigations are performed at the High-field MR-center on on-site available materials for 3D printing. This research aims at finding out if easily available solid materials are also MR-visible.

A selection of materials, with different solidity, is made to investigate their MR visibility properties (Figure 3.2):

- Soft materials : silicone types.
- Hard materials : filaments and printed objects with PMMA or polylactic acid PLA (common used polymers for FDM 3D printers) and Poly(vinyl alcohol) PVA (often used for support during 3D printing).

The shape might have an impact on the B-field if the material features susceptibility differences to surrounding air or liquids or other materials. Therefore thin and thicker type of samples are investigated, like for example a thin silicon model (the vessel, right on figure 3.2) and a thicker one (the heart, left on figure 3.2).

Moreover, a resolution phantom for MR has been produced by computer-aided design (CAD). The phantom is a set of 6 cubes with a grid pattern (period of 4,5) with decreasing size: from 2,5cm length to 0,4mm. The design of such a 3D grid phantom has been

proposed already in 2015 for Quality Assurance (QA) on best performing 3D printers and high resolution MRI [Berg, 2015]. For this master thesis, it has been 3D printed with PLA using the Ultimaker3 printer available at the High-field MR-center.

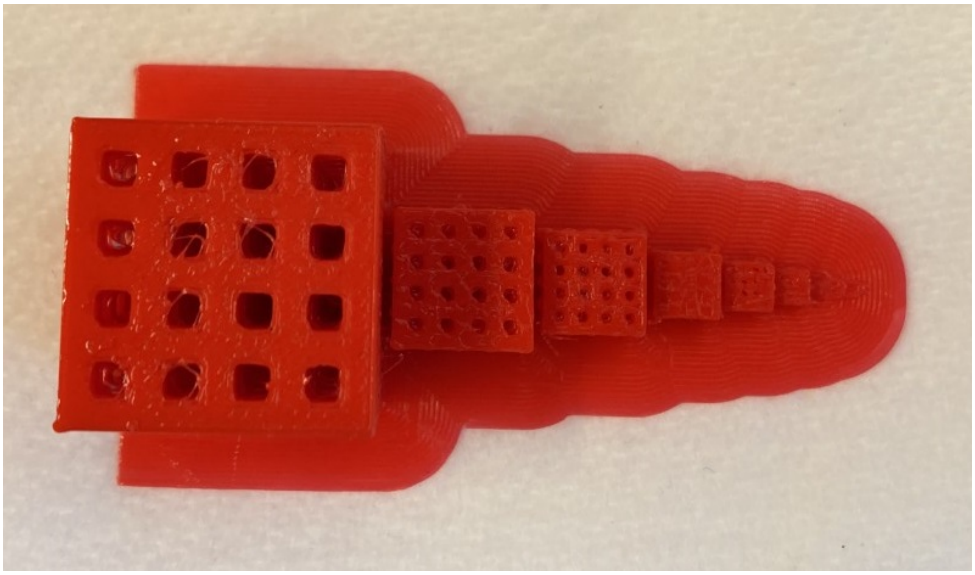

Figure 3.3: MR resolution phantom composed of 6 cubes with a grid pattern (3D printed using PLA)

3.2 MR visible polymer : Patent EP 3974903

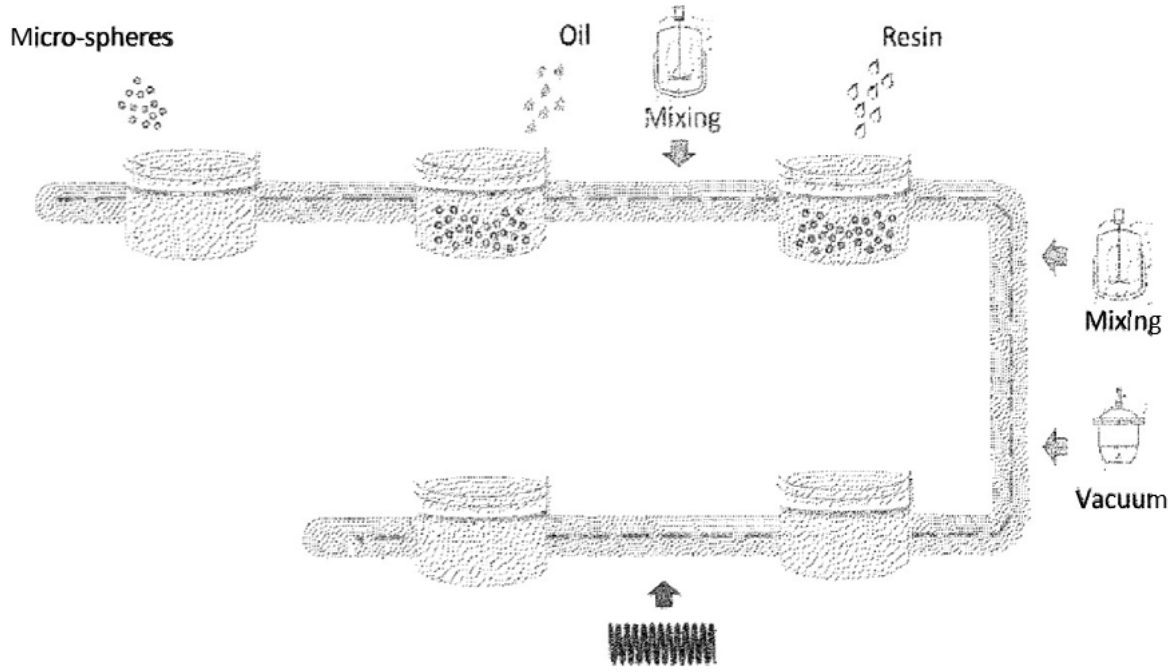

Figure 3.4: Scheme presenting the major steps of the patented manufacturing process for producing MR-visible solid resin with micro-spheres. [Rausch et al., 2022]

The main samples used for this master thesis are manufactured at CMPBME (Medical University of Vienna) by Markus Ortner, member of the project. The producing method has been patented in the European Union (Nr. EP 3974903).

The goal of the manufacturing process is to provide a reproducible mixing procedure for homogeneous MR-visible solid polymers. The samples are composed of three major constituentss in order to reach the desired properties of MR-visible solid polymers:

1. **MR signal producing liquid** : Due to the high mobility of protons the used fluid is responsible for the generation of an MR signal. Different liquids can be used to generate multiple samples with different T1 and T2 values and therefore different contrast. The liquids used for this master thesis, mainly oils, are discussed below.
2. **Micro-particles** : Two types of micro particles are investigated, micro-spheres and micro-capsules. They are responsible for absorbing the liquid while retaining its mobility property in a certain amount in order to produce an MR signal. "The ratio between the particles and the used fluid can be adjusted to obtain different MR signal and contrast properties." [Rausch et al., 2022]

3. **Light-curable resin** : Through UV exposition the resin hardens leading to a solid material at the final end. A photo-polymer is used to offer also the possibility to be used by means of three-dimensional lithography-based additive production.

The production steps are presented figure 3.4. Because three elements compose the samples, three major steps are required :

1. Adding the magnetic resonance imaging-signal producing liquid to the micro-particles.
2. Mixing the filled particles with a light-curable resin.
3. Solidification through UV-light exposure.

3.2.1 Proton-rich liquids

In order to obtain an MR signal, proton-rich fluids are chosen. The goal is to obtain multiple range of contrast by varying T1 and T2. Mainly oils are investigated, but it is expected that any other liquid, like water, could be used. They are presented table 4.4.2

Table 3.1: Proton-rich liquids

Liquid	Industrial name	Viscosity [cSt]
Water	-	1
Standard paraffin oil	Paraffinum perliquidum (CAS 8042-47-5)	33.5
Standard silicon oil	ELBESIL ÖLE B10	10
Standard silicon oil	Silikonöl SF-V50	50

MR measurements of the liquid oils are performed using the same protocols as for the solid resins (described in the next section). The results for T1, T2 and T2* are presented in table 4.4.2. They serve as reference measurements for comparison with the manufactured solid samples.

Table 3.2: T1 values for the proton-rich liquids used

Oils	T1- VFA	T1 - 2D PSR	T1 - IR
Paraffin oil	174.7 ± 9.9	168.7 ± 1.7	188.6 ± 0.8
Silicon oil 10 cSt	1450.8 ± 217	1116.8 ± 183.7	1235.9 ± 9.6
Silicon oil 50 cSt	1150.1 ± 47.9	949.2 ± 59	1097.3 ± 10.4

Table 3.3: T2 values for the proton-rich liquids used

Oils	T2	T2*
Paraffin oil	95.0 ± 0.5	2.9 ± 0.7
Silicon oil 10 cSt	981.0 ± 31.3	29.3 ± 4.6
Silicon oil 50 cSt	602.0 ± 7.9	8.9 ± 0.9

3.2.2 Micro-spheres

The micro-spheres used are the porous Techpolymer, cross-linked polymethylmethacrylate spherical particles. Techpolymer MBP-8 is available from Sekisui Kasei Co., Ltd, and the micro-spheres are found as powder in their initial state. According to the patent for the manufacturing process, the micro-spheres"have a "specific surface area of 60-100 m^2/g", and the pores of the particles have a "mean diameter of 150-250 Å" [Rausch et al., 2022].

Figure 3.5: Samples MS007, MS008, MS009 (from left to right) are manufactured with micro-spheres and paraffin oil. They are moulded discs of 10cm diameter and approximately 2.2cm height.

A total amount of 200g of mixture is prepared. The final weight of the samples is measured after removing the residual oil on the surface of the samples.

The preparation with micro-spheres is divided into three sets of different contrast liquid concentration, in order to investigate the influence of this manufacturing parameter on the MR-signal obtained. Each set is composed of three samples to control the repeatability of the manufacturing process (figure 3.5):

- Reference samples, manufactured with 30g of contrast liquid
- Samples with +15% concentration, manufactured with 34.5g of contrast liquid
- Samples with −15% concentration, manufactured with 25.5g of of contrast liquid

3.2.3 Micro-capsules

Another type of micro particles is being used in the manufacturing process: the micro-capsules.

The micro-capsules differ from the micro-spheres as they are directly produced by mixing oil resin and surfactant to decrease the surface tension between the two first components. They are then hardened and dried to form a powder, which is finally mixed with more resin to manufacture the sample. Different sizes of micro-capsules can be produced (1mm ; 0,5mm ; 0,1mm) by changing the proportion of the mixture components and by filtering the obtained powder with a sieve.

The challenge is to ensure that the contrast liquid is well encapsulated. Therefore, even though the process tends to be systematic, probes may vary from one another. (figure 3.6)

Figure 3.6: Samples MC003 and MC004 are manufactured using a mixture of micro-capsules with paraffin oil within a molding process with UV hardening in liquid rezin.

3.2.4 3D printing strategy

Finally, to obtain a solid material, the micro-spheres or the micro-capsules are mixed with a light curing resin. Two main resins are used the Anycubic Resin Standard Plus, Clear, UV wavelength 405nm (Shenzen ANYCUBIC Technology CO., Ltd).

The probes with micro-spheres are moulded in discs with a diameter of $10cm$ and height of $2.2cm$. The micro-capsules are moulded in slabs with varying height.

The manufacturing process aims also to be compatible with 3D printing. The first tests for 3D printing are performed with the micro-capsules and a Digital Light Processing (DLP) 3D printer like the Form3 (Formlabs GmbH, Germany). The first 3D printed samples are cubes of height $3cm$, shown in figure 3.7.

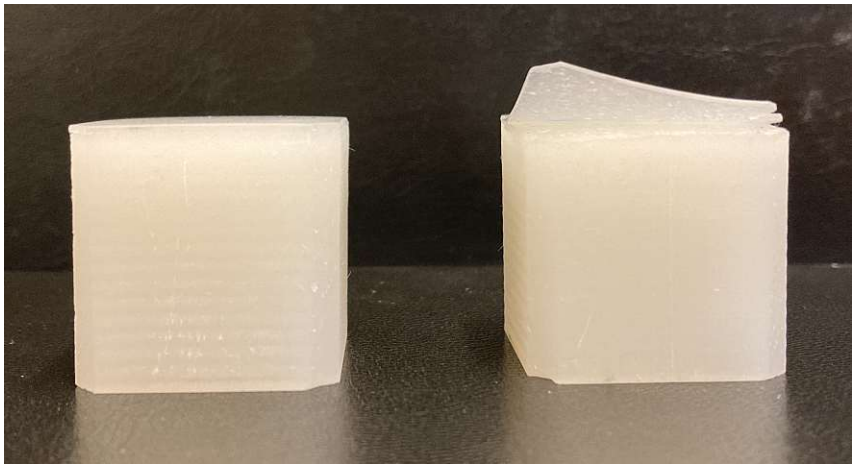

Figure 3.7: 3D printed samples MC005 and MC004 manufactured with micro-capsules and paraffin oil.

Already after their production a difference can be perceived between the samples. They are opaque, with different color according to the contrast liquid used : yellowish for the paraffin oil and white for the silicone oil. The outer surface of the samples looks homogeneous. Magnetic resonance imaging has the advantage to be non invasive and to provide different parameters for contrast. Therefore the inner part of the samples can be imaged and its homogeneity assessed, without damaging it. After every measurements, it is crucial to keep the manufacturer, Markus Ortner, involved and provide him with a feed-back on the samples.

3.3 3T MRI scanner

Imaging experiments of the printed samples are performed on a whole-body 3T Prismafit scanner (Siemens Haelthineers, Erlangen/ Gemany) available at the High Field MR-Center of the general hospital of Vienna. It is an MRI scanner conceived for both research and clinical applications.

For radio frequency (RF) signal reception a 15-channel phased array knee coil is used.

Room temperature is also measured for each scan, varying between 20°C and 21°C, as T1 and T2 depend on temperature..

Figure 3.8: 3T Prismafit MRI scanner at the High field MR-Center

Table 3.4: MRI characteristics

MR parameters	Protocol
Static magnetic field	$B_0 = 3$ T
Dynamic magnetic field gradient system	G = 70 mT/m
Bore diameter	60 cm
Maximum FOV	50 cm.

3.4 MRI sequences

3.4.1 Measurement protocol

The printed samples have to be assessed by mean of relaxation times on on-site available MRI systems using standard contrast weighting MR-methods. The protocols are chosen in order to obtain a T1 map, a T2 map and a T2* map of the samples.

The samples have been placed in stacks at the center of the 15ch knee coil. To ensure reproducible positioning, the coil is centered on the MRI table using a LASER. Then the scanner aligns it automatically at the iso-center, i.e the center of the magnetic field and gradient system for optimum usage of the FOV. T2 relaxation times can be measured using a routine spin echo pulse sequence, consisting of subsequent rf- and magnetic field gradient pulse (pulse sequence). For T1, the sequence that provides the best compromise between precision and scanning time has to be chosen. Therefore three sequences are investigated in this project to measure T1 : the inversion recovery sequence (IR), the variable flip angle sequence (VFA) and the progressive saturation recovery method (PSR). The established protocol for investigation and quality control of the samples is composed of the following sequences :

1. Free Induction Decay (FID),
2. Localizers,
3. 3D Gradient Echo (3D GRE),
4. Ultra-short Time Encoding (UTE),
5. Inversion Recovery (IR),
6. Progressive Saturation Recovery (PSR),
7. B1 map
8. Variable Flip Angle (VFA),
9. Carr-Purcell-Meiboom-Gill (CPMG),
10. 3D GRE for T2* mapping.

First the MR scanner has to be calibrated to ensure the precision of the measurements. The resonance frequency is set up (ex : f=123251450 Hz) and the flip angle adjusted. In fact, this step of transmitter gain/attenuation adjustments is required as we need to ensure for each measurement a proper calibration of the RF pulse to achieve a 90° flip angle [Elster, 2023]. We then adjust power until it converges, which allows to fix a reference

voltage. In the performed scans the reference voltage is 130V. 3D shimming using linear and non-linear space dependent magnetic field components (shim) is then operated to adjust the homogeneity of the magnetic field. The protocol used on the 3T scanner for automatic shimming is the GRE prostate protocol, with a low receiver gain. If the phase variation is small it means that the shimming is good. After shimming the transmitter frequency must be adjusted again. Right after these FID adjustment steps, a 'localizer' sequence is started. It is "a set of three low-resolution, large field-of-view localizers in each plane used for orientation" [Bogaert et al., 2019] and for selecting the Field-of-View (FOV). The goal is to visualize where the samples are located. It enables to accurately adjust the field of view, the distance factor, the number of slices and the slices per slab in the following sequences. Sagittal, coronal and axial cuts are obtained and displayed on the command window.

3.4.2 Gradient Echo (GE)

In the protocol, two gradient echo sequences are used. First, for judging on visibility, inhomogeneities and irregularities in manufacturing of the MR visible resin a 3D gradient echo (3D GRE) sequence with high resolution (0.9 mm) is applied before starting T1 and T2 measurements. The gradient echo sequence is also used to assess T2*. In this case, it is a 2D sequence which is performed, with slice selective selection for avoiding un-folding artefacts in the measurement.

A Turbo Spin Echo (TSE) sequence and a Gradient Echo (GRE) sequence with no spoiling generates stimulated echoes from series of 90° RF-pulses repeated at time interval, called repetition time (TR). No 180° rf-rephasing pulse is needed for a GRE sequence[1]. In general, gradients for slice selection, frequency and phase encoding dephase the spins at different positions. To compensate for this phenomenon, the slice selective gradient is followed by a negative gradient of half of its size. The negative phase adds to the dephased spins which become in phase again. Furthermore, the readout gradient (frequency encoding) is also preceded by a negative gradient which will compensate for the phase shifts of the positive readout gradient (figure 3.9). Finally, during the readout gradient, when all spins are aligned again (phase equal to zero) a gradient echo is produced. The gradient

[1]Berg, A. (2021). Postgraduate University Course: "Medical Physics", lecture handouts: Magnetic Resonance 1; Medical University of Vienna, WS 2021/2022

echo decay can be mathematically described by the following equation [Reiser et al., 2007]:

$$M_z(TE) = M_0 e^{-\frac{TE}{T2^*}} \tag{3.1}$$

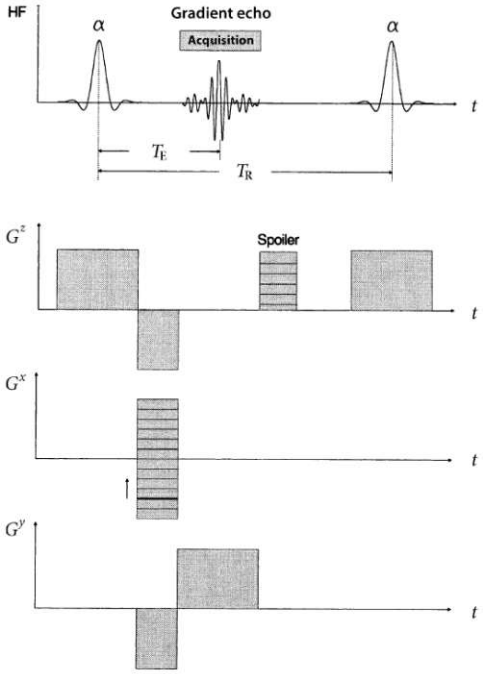

Figure 3.9: Gradient echo sequence scheme [Reiser et al., 2007]

T2* maps can be obtained by acquiring images at different echo times (TE) and fitting the data from the resulting images to equation (3.1). T2* is however very sensitive to magnetic field inhomogeneities.

Table 3.5: 2D GRE sequence protocol for T2* mapping

MR parameters	Protocol
Repetition time (TR)	2000 ms
Echo time (TE)	3.51, 11.9, 34.6, 57.3, 80 ms
Slice thickness	0.9 mm
FOV	120 mm
Matrix size	128*128
Voxel size	$0.9 * 0.9 * 5.0 mm^3$
Pixel bandwidth	698 Hz
Acquisition time	12min56

TR is adjusted to the samples: long TR (ex: 6000ms) for samples with long T1, shorter for samples with shorter T1.

3.4.3 Ultra-short Time Encoding (UTE)

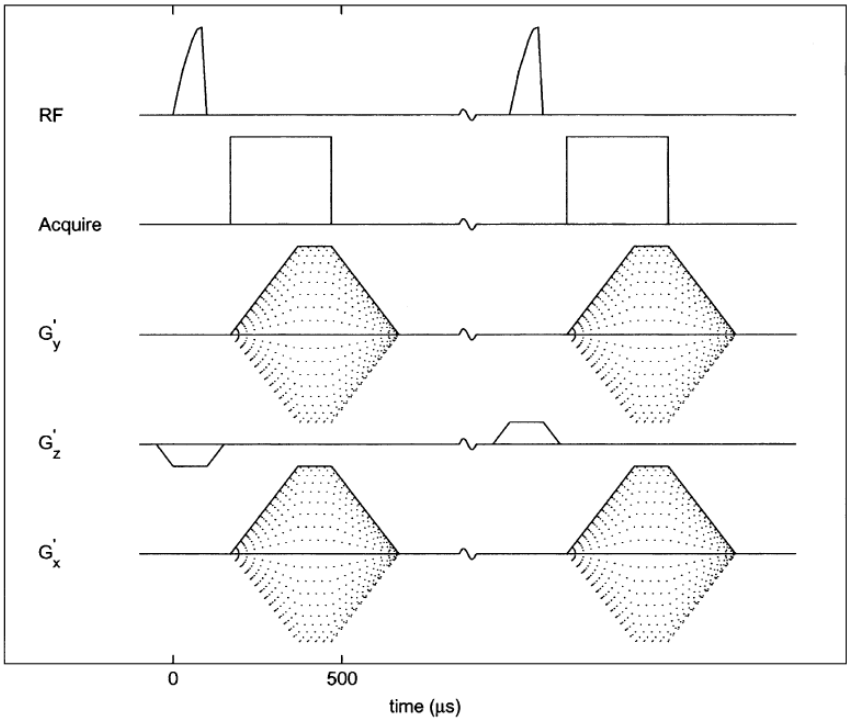

Figure 3.10: UTE sequence [Holmes and Bydder, 2005]

Polymer materials are known to have very short T2. The consequence is a very quick decay of the MR signal. Therefore the standard used echo times (TE in the range of ms) are too long for acquiring signal from solid materials, resulting in dark images.

The goal of Ultra-short echo time imaging (UTE) is therefore to drastically reduce TE from about 2 ms to about TE = 0,05 ms. With short TE, a signal can be produced and materials with short T2 can be observed.

UTE uses for this purpose half radio-frequency (rf) excitations with radial mapping from the center of k-space. [Robson et al., 2003]

In the protocol, a UTE sequence is used during the first measurement of new samples for visualization. It allows to investigate samples producing little or no signal in the 3D gradient sequence.

3.4.4 Inversion Recovery (IR)

The inversion recovery sequence is the gold standard method for acquiring precise T1 maps. The sequence starts with a 180° pulse, which inverts the longitudinal magnetization from its equilibrium status. After a defined time, called "inversion time" (TI), a 90° pulse is newly applied in order to rotate the partially relaxed longitudinal magnetization. Finally, the last step is the readout sequence, which can be either a spin-echo or a gradient-readout. The pulse scheme for inversion recovery is therefore: 180° - TI 90° - Acquisition (figure 3.11).

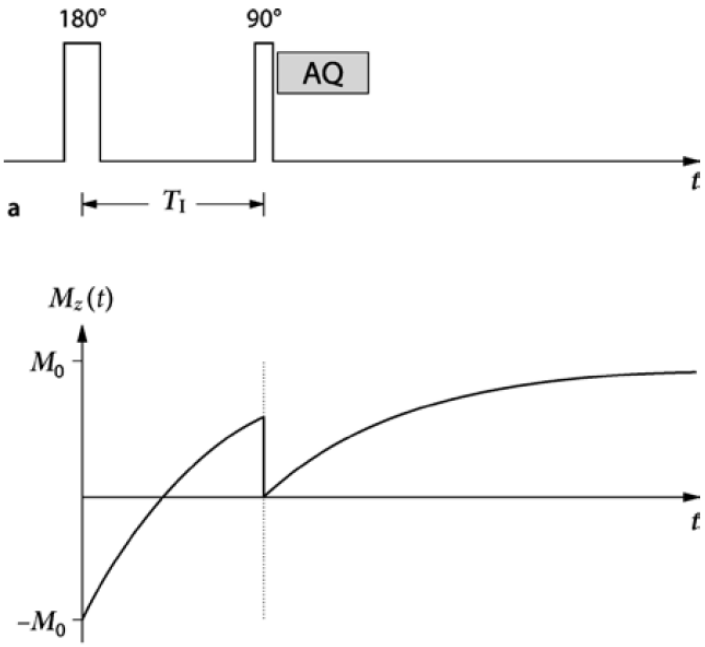

Figure 3.11: Inversion recovery sequence [Reiser et al., 2007]

By acquiring signal at different inversion times the signal recovery curve can be reconstructed and then fitted in order to obtain T1. The acquired signal can be then modelled by the Bloch equation, expressing an increased change in the longitudinal magnetization, in comparison to the saturation recovery sequence [Boudreau, 2023]:

$$M_z(TI) = M_0(1 - 2e^{\frac{TI}{T1}}) \tag{3.2}$$

If the experiment is performed with long enough repetition times (TR), approximately 5 times T1 ([Steen et al., 1994]), the longitudinal magnetization has time to fully relax.

The data fitting procedure is a major challenge as due to the 180°-flip. The longitudinal magnetization is inverted at the beginning and has negative values. Two possibilities exist for the data fit:

- Polarity inversion if magnitude images are obtained.
- Phase sensitive data fit

In this master thesis the program qMRlab is chosen for post-processing the data, using polarity inversion. This open source MATLAB code performs within a specific module for IR, "inversion_recovery: Compute a T1 map using Inversion Recovery data", a 3-parameter model by using a reduced-dimension non-linear least squares (RD-NLS) algorithm. [Barral et al., 2010b] Moreover, the whole sequence is composed of the multiple repetition of this inversion 180° pulse. A long TR, to ensure full relaxation before each inversion pulse is used in order to acquire several data points. The drawback of this method is the increased measurement times.

T1 relaxation time measurements are performed using a 2D single-slice inversion recovery (IR) turbo spin echo (TSE) sequence. The scan is composed of 12 repetitions of the same pulse sequence with different TI protocol parameter. For T1 mapping, 12 inversion times are selected to cover the range of the longitudinal relaxation of the samples. The total acquisition time (TA) is approximately 32 min.

Table 3.6: IR sequence protocol

MR parameters	Protocol
Inversion Times (TI)	25, 50, 100, 150, 250, 500, 1000, 1100, 1500, 2500, 3000 ms
Repetition time (TR)	7000 ms
Echo time (TE)	5.4 ms
Slice thickness	0.9 mm
FOV	120 mm
Matrix size	128*128
Voxel size	$0.9 * 0.9 * 5.0 mm^3$
Turbo factor	6
Pixel bandwidth	710 Hz
Acquisition time	33 min

In order to reduce the acquisition time which might be problematic for clinical use, two other sequences are investigated for T1 quantification with reduced measurement times.

3.4.5 Progressive Saturation Recovery (PSR)

Reducing scanning time is relevant. Therefore the second sequence investigated is the Progressive Saturation Recovery sequence.

The sequence is based on the pulse scheme 90°-Acquisition-TR. First a 90° rf-pulse excites the initial z-magnetization, which is then relaxing to thermal equilibrium (Mz0) according to the sample specific T1.

After the recovery time TR the next 90° pulse is applied. Only the recovered z-magnetization, is flipped to the xy-plane, where it can be detected as FID. [Reiser et al., 2007]

The scan is performed for different repetition times : TR= 512, 256, 128, 64, 32, 24 ms. At each repetition time a point of the T1 relaxation curve is obtained. The acquired images for these repetition times will be used to be fitted in the corresponding model [Kingsley, 1999]:

$$M = M_0 \cdot (1 - e^{-\frac{TR}{T1}}) \tag{3.3}$$

The influence of adding offset on the fit, $M = M_0 \cdot (1 - e^{-t/T1}) + M_{offset}$, will be further investigated.

2D slice selection sequence has been selected instead of a 3D sequence, in order to reduce aliasing and infolding artefact.

Table 3.7: 2D PSR sequence protocol on the 3T Prisma fit scanner

MR parameters	Protocol
Repetition time (TR)	24, 32, 64, 128, 256, 512, 1024, 2050 ms
Echo times (TE)	2 ms
Slice thickness	0.9 mm
FOV	120 mm
Matrix size	128*128
Voxel size	$0.9 * 0.9 * 5.0 mm^3$
Echo train length	6
Pixel bandwidth	700 Hz
Acquisition time	10min4

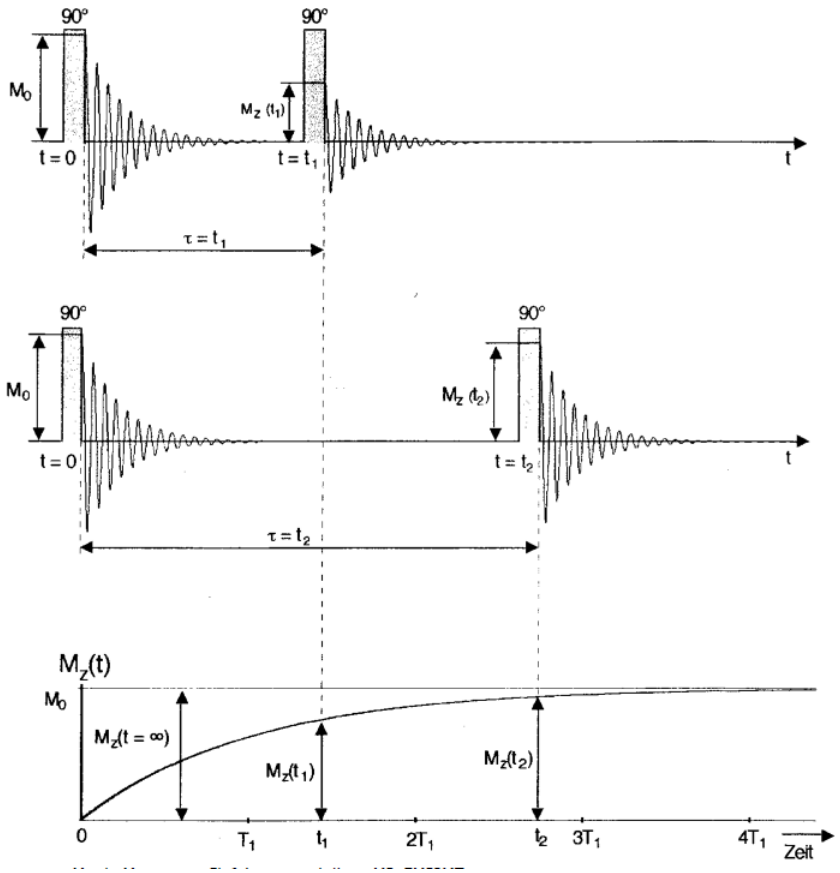

Figure 3.12: Progression saturation recovery sequence[2]

The protocol needs to be adapted for the type of contrast liquid, which is used in manufacturing of the MR visible resin, by increasing the repetition times for long T1 samples or decreasing it for shorter T1 samples.

[2]Meyerspeer, M. (2021). "Einführungspraktikum MR", lecture handouts; Medical University of Vienna

3.4.6 Variable Flip Angle (VFA)

The Variable flip angle sequence is finally also investigated in order to compare its results to the inversion recovery sequence and the progressive saturation recovery sequences. The two previously described sequences have the disadvantage that they require measurement of equilibrium magnetization. Therefore the scanning time is increased as long TR have to be used to ensure sufficient recovery after a 90° pulse.

The variable flip angle (VFA) method is an MR sequence which allows rapid 3D T1 mapping. The idea is to flip the longitudinal magnetization (Mz) at different angles shorter than 90°. For each flip angle a spoiled gradient echo is acquired, which allows to then deliver a T1 value. [Fram et al., 1987]

VFA requires shorter acquisition times, as it uses shorter repetition time, in the order of 10 to 50ms. Using shorter flip angles allows to reduce the TR time, by the cost of a partly saturated, i.e. lower signal. If for the first relaxations the longitudinal magnetization tends to decrease, after several cycles Mz reaches a stable value, corresponding to an equilibrium between the flip and the relaxation phenomena. This constant value for Mz corresponds to the so called "steady-state". The latter signal is maximized for a specific angle called the Ernst angle [Ernst and Anderson, 1966] :

$$\theta_{Ernst} = \arccos(e^{-\frac{TR}{T1}}) \tag{3.4}$$

The sequence is shown figure 3.13

Before each new excitation flip a spoiling is performed in order to avoid rest magnetization in the transverse plane. Indeed, by working with short repetition times the transverse magnetization (Mxy) might have not enough time to disappear completely.

The steady-state longitudinal magnetization is described by the Bloch equation for the spoiled gradient pulse sequence, at ideal flip angle and repetition time TR. [Fram et al., 1987]

$$I(\theta) = \frac{N(H)(1 - e^{-\frac{TR}{T1}})\sin\theta}{1 - (e^{-\frac{TR}{T1}}e^{-\frac{TR}{T2*}}) - \cos(\theta)(e^{-\frac{TR}{T1}} - e^{-\frac{TR}{T2*}})} \tag{3.5}$$

N(H) is the proton density and θ is the RF excitation pulse flip angle.

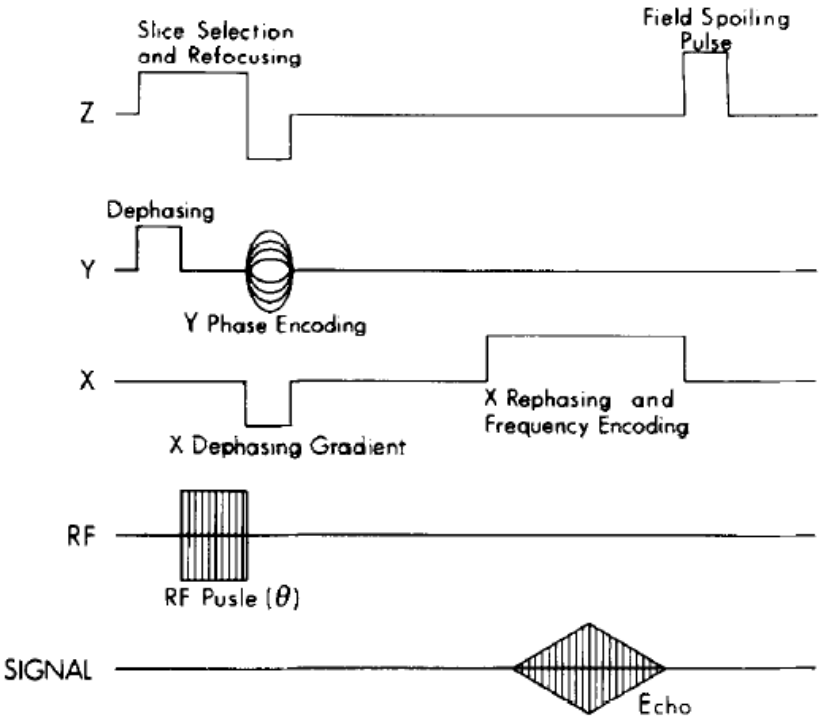

Figure 3.13: Variable flip angle sequence [Fram et al., 1987]

By rearranging equation 3.5, T1 can be derived from a linear equation fit.

$$\frac{I(\theta)}{\sin\theta} = e^{-\frac{TR}{T1}}\frac{I(\theta)}{\tan\theta} + N(H)(1 - e^{-\frac{TR}{T1}})e^{-\frac{TE}{T2*}} \tag{3.6}$$

A linear regression, calculated with $\frac{I(\theta)}{\sin\theta}$ and $\frac{I(\theta)}{\tan\theta}$ values, gives a straight line. From its slope a, T1 can be derived :

$$T1 = -\frac{TR}{\ln a} \tag{3.7}$$

However, equation (1) comes with several assumptions, which have an influence on the obtained T1 value:

- "longitudinal magnetization has reached a steady state after a large number of TRs
- transverse magnetization is perfectly spoiled at the end of each TR." [Boudreau, 2023]

Moreover, the VFA sequence is also very sensitive to inaccuracies of the flip angle. [Baudrexel et al., 2018] Due to many perturbation factors, the chosen flip angle on the scanner console often differs from the real flip angle experienced by the spins. For homoge-

neous signal intensities a homogeneous transmitter intensity (B1) is necessary. Therefore, before each T1 mapping sequence a B1 map has to be performed. [Boudreau et al., 2017] B1 designs the transmitted RF amplitude, which is responsible for the flip of the spins. In most of MRI coils there are B1 inhomogeneities. The variable flip angle method is very sensitive to these inhomogeneities which might lead to systematic error in the T1 values. Performing a B1 map allows then to calibrate the nominal flip angle to its actual value. The nominal flip angle is corrected voxelwise by a scaling factor obtained for the latter B1 map.

Table 3.8: Variable flip angle sequence protocol on the 3T Prisma fit scanner

MR parameters	Protocol
Flip angles	5°, 12°, 18°, 24°, 29.9°
Repetition time (TR)	50 ms
Echo times (TE)	2.76 ms
Slice thickness	4.0 mm
FOV	160 mm
Voxel size	0.4*0.4*4 mm
Matrix size	224*160
Echo train length	6
Pixel bandwidth	300 Hz
Total acquisition time	4min45

An MR-protocol for measuring the B1 distribution is available on the clinical MR-scanner. On the 3T Prisma Fit scanner from Siemens, the sequence for B1 mapping sequence is linked to the VFA. The Siemens software Syngo delivers directly the corresponding T1 map. Five flip angles are selected and the repetition time is adapted to the type of samples. For samples with long T1, TR=50ms, which increases the total scanning time. For samples with shorter T1, TR=2ms.

3.4.7 Carr-Purcell-Meiboom-Gill (CPMG)

T2 quantification is of significant interest as it delivers information about the mobility and chemical environment of a medium. It is therefore a good characteristic of the medium.

In order to assess its value a standard multi-echo sequence is performed. This sequence is based on the principle of the classical Hahn spin echo [Hahn, 1950]. Excitation is induced by a 90° pulse resulting in a decay of the signal (FID). Then a refocusing pulse of 180° is sent. The consequence of the latter is that the slower precessing spins are now in advance to the faster ones. When the fast precessing spins catch up again the slower precessing ones the net magnetization builds up again and an "echo"-signal is observed (spin echo). [Mansfield, 1982]

The Carr-Purcell-Meiboom-Gill (CPMG) sequence is a multi-echo sequence. It improves the CP sequence by using different excitation rf-phases for the 90° excitation pulse (e.g. b1 along x' axis and a 180° rf pulse along y' axis), which results in a partly compensation of imperfect 180° rf-pulse [Carr and Purcell, 1954].

For each echo time we obtain an image of a slice with the corresponding T2-weighted signal intensity. These intensity values related to the echo time can then be used to obtain T2 by fitting a decaying exponential to the dataset. The spin-echo signal M can be described by the following equation, T2 being the characteristic time [Reiser et al., 2007]:

$$M = M_0 \cdot e^{-t/T2} \tag{3.8}$$

Table 3.9: CPMG sequence protocol on the 3T Prismafit

MR parameters	Protocol
Repetition time (TR)	2000 ms
Echo times (TE)	10,20,30,40,50,60,70,80,90,100 ms
Slice thickness	0.9 mm
FOV	120 mm
Matrix size	128*128
Voxel size	$0.9 * 0.9 * 5.0 mm^3$
Echo train length	10
Pixel bandwidth	700 Hz
Acquisition time	12min

The echo times TE are adjusted to the corresponding type of contrast being used. For paraffin oil as T2 is around 100ms, in order to obtain a good fit TE = 10, 20, 30, 40, 50, 60, 80, 90, 100ms. Whereas for the silicone oil, which has a higher T2, the echo times are increased to optimize the fit : TE = 20, 40, 60, 80, 100, 120, 140, 160, 180, 200ms.

The repetition time is also adjusted to the corresponding contrast liquid as we need a full relaxation before sending the new pulse. Therefore for paraffin oil TR=2000ms and for silicone oil TR=6000ms.

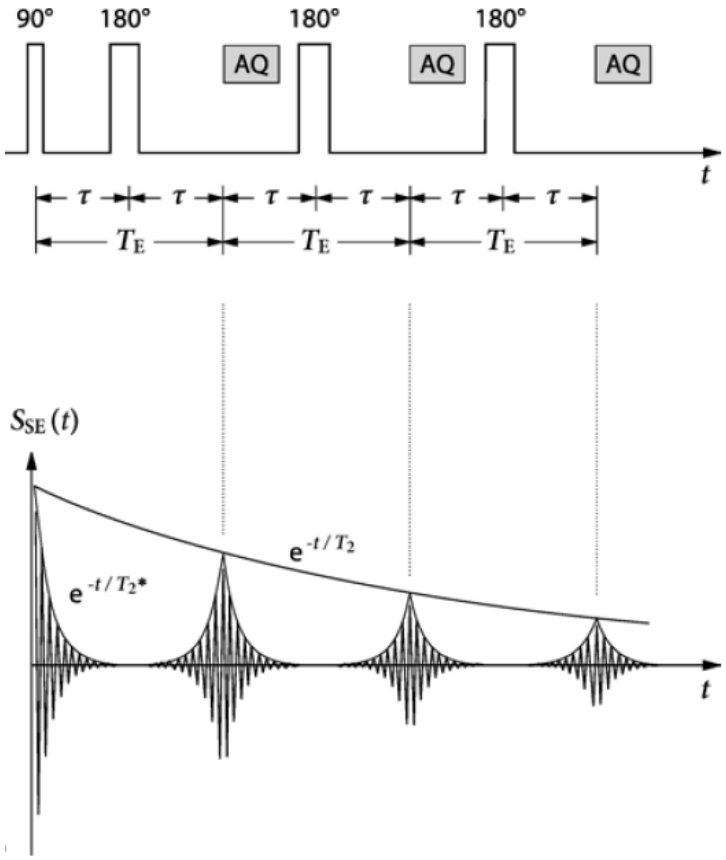

Figure 3.14: CPMG sequence (top) and corresponding signal curve (bottom) [Reiser et al., 2007]

3.5 Image processing

3.5.1 Multi-slice fit

In order to assess T1, T2 and homogeneity of the samples the data extracted from the MR scans are analysed using different image processing software:

1. *SYNGO* provided by Siemens is used for quick visualization of imaging results, measurement of spatial distances and DICOM parameters.
2. *MATLAB* is used for coding a multi-slice fitting routine to obtain a T1 and T2 map, and removal of first echoes for avoiding inaccuracies related to stimulated echoes.
3. *qMRLab* is a MATLAB package used for quantitative assessment of T1 using the inversion recovery method.
4. *ImageJ* is finally used for quantitative analysis of the T1 and T2 maps on selected regions of interest (ROIs).

The data acquired by MRI are saved in DICOM format, accordingly to the sequence performed. First using SYNGO the data are classified in different folders corresponding to the MR sequence.

The MATLAB routines for T2 and T1 mapping are based on exponential fits performed for each pixel using the T1-weighted and T2-weighted images from the scans at different echo times (T2 map) or repetition times (T1 map) as it will be explained in the following part.

The T2 mapping routine requires a slice selection and the first echo has to be removed for avoiding stimulated echo artifacts. [Milford et al., 2015] The latter shows reduced intensity due to the impact of stimulated echoes. If it is not removed, the first data point in the echo sequence exhibits a reduced signal intensity with comparison to the second. The exponential fit is then highly impacted and will result in an inaccurate T2 value above the one more correctly obtained.

The first step is therefore to order the multiple files of the multi-echo MRI sequence. The files for each slices have to be organized in stacks ordered by the echo times, ranging from the shorter echo time to the longest. This is the step where the first echo slice can be removed by not integrating it into the stack.

Then DICOM files are read with the MATLAB function "dicomread()". They are afterwards concatenated in order to give M x N x nEchoes x nSlices matrix, where M is the length and N the height of the image (often 128x128 in our case). [Birkbeck, 2023] There is for each slice a matrix at a specific echo time, filled with numbers corresponding to the intensity of the signal for this precise echo time.

The user has to enter as input:

- The number of slices
- The number of echoes
- The choice to include or not the first echo
- The corresponding echo times
- The slice selection

Each pixel of the image represents an intensity value. This intensity depends on the echo time. For each slice we have therefore as many images, with different intensities, as echo times. In order to construct a T2 map of a slice, for each pixel the different intensity values have to be fitted into the equation corresponding to the parameter selective (T2 or T1) pulse sequence. In the case of CPMG sequence it is a decaying exponential, with T2 as fitting parameter: equation (3.8)

The fit consists in solving a nonlinear curve-fitting (data-fitting) problem with minimizing of the squares of the differences between the measured data points and the fitting curve ("least sqaure fit"). For this purpose the MATLAB function "lsqcurvefit" is used, which is a nonlinear least-squares solver. The function to fit is in MATLAB the anonymous function $fun = @(x, xdata)x(1) * (exp(-xdata/x(2)))$.

In order to reduce the calculation time dependent on the loop on each pixel of the 128 by 128 matrix a "parfor loop" is used, which operates several loops in parallel. Moreover the initial parameters are chosen in order to be close to the results according to precedent results obtained without first echo removal on ImageJ. These are the starting value and the min and max limits.

The resulting T2 map is then converted into a format on 16 bits (.tiff) in order to be read and quantitatively processed on ImageJ. The T2 map is also displayed with the possibility to choose a pixel and display the corresponding exponential fit.

These MATLAB routines have a problem in terms of processing time. As the loop is performed on each pixel, the processing time increases strongly with the Matrix size.

The MATLAB routine for the T1 map follows quite the same procedure but with its own specificity. Actually the first step is also to organise the files into stacks but this time ordered according to their repetition time and without removing the first echo/slice. They are also concatenated afterwards in order to give a multidimensional Matrix:
M x N x n repetition times x n slices. There is for each slice a matrix at a specific repetition time, representing the intensity of the signal for this precise repetition time. Similar to T2-evaluation the user has to choose inputs: "Number of slices", "Repetition times", "Taking or not the offset", "Slices" to be analysed.

T1 fitting is performed, similar to T2, with the MATLAB function "lsqcurvefit". The main difference here is the function which is used for fitting the function graph to the data. Indeed in the case of a progressive saturation recovery sequence the function to be fitted is an increasing exponential, corresponding to the function (3.7), which is written in MATLAB with the anonymous function $fun = @(x, xdata)x(1)*(1-exp(-xdata/x(2)))+x(3)$. It is a two or three parameter fit as there is in this case the possibility to add an offset or not to the exponential fit. Indeed it has been noticed in the plots obtained that adding a non-zero offset fitting parameter the fit significantly improved (figure 3.15). Finally the T1-map is stored on 16 bits in a ".tiff" format for further analysis with ImageJ.

The MATLAB package qMRLab [Karakuzu et al., 2020] is used to assess T1 by mean of the inversion recovery sequence, with the specific module " inversion_recovery: Compute a T1 map using Inversion Recovery data" [Barral et al., 2010b] For this purpose the DICOM data from the IR scan are converted into the NIFTI format for integration in qMRLab. This is done using a MATLAB package: "Siemens DICOM sort and convert to NIfTI".[Robinson, 2023] For each inversion time a NIFTI file of the corresponding slices is created. The latter are then stacked according to their inversion times into one single file. This stack is finally implemented into qMRLab, which delivers the resulting T1-map and fitting curve. The data are fitted according to a polarity inversion.

The input parameters for the fit are:

- the inversion time
- the recovery time
- the slice to be analysed

3.5.2 T1- assessment

For each slice of the sample, three T1-maps are obtained : one directly from the Siemens scanner for the variable flip angle and two other ones from the MATLAB routine for the PSR and the IR sequence. The obtained T1 maps are then loaded into ImageJ for quantitative assessment of T1 in selected ROIs. A region of interest (ROI) consisting of a circle or a rectangle depending on the geometry of the sample is selected. The ROI is designed to be as large as possible avoiding the border rim of the sample with distortion and inhomogeneity artifacts.

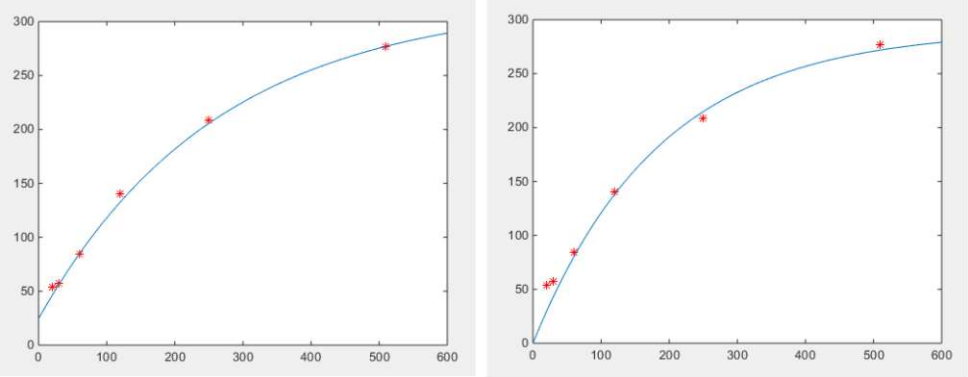

Figure 3.15: Plot of the exponential fit with offset (left), $M_z = M_0 \cdot (1 - e^{-t/T1}) + M_{offset}$, and without offset (right), $M_z = M_0 \cdot (1 - e^{-t/T1})$, for one pixel of the sample MS010. When taking into account the offset the T1 value is significantly increased (T1(offset) = 227.3 ± 10.8 ms vs. T1 = 171.1 ± 9.1 ms) demonstrating the high sensitivity of the calculated values for fitting parameters on the number of pre-selected fitting parameters.

The quality of the fit for the progressive saturation recovery sequence can be visually qualified by plotting the exponential fit: figure 3.15. The comparison between the results with offset and without offset shows a better fit when taking into account the offset. The physical-mathematical reason for this offset initially had been unclear and has been investigated furthermore. It has been found that the offset is not related to noise due to an amplifier, by comparing the fit offset values with the background noise signal. The hypothesis is therefore that the offset is partly determined by non-spoiled rest magnetization.

3.5.3 T2- and T2*- assessment

As for T1, the T2 maps obtained with MATLAB for the different slices of each measured samples are evaluated with a ROI analysis in ImageJ. Slices for evaluation are selected such that only slices completely located inside of the samples are considered. Indeed slices on the borders of the samples present a high level of inhomogeneities and cannot be processed. A circular region of interest is then selected in order to cover the maximum pixel area of the slice. The mean value of T2 for this ROI is calculated as well as the standard deviation. If there are multiple operable slices for the same sample the calculation is repeated trying to keep the same ROI. The mean value of T2 for the different slices is reported as the relaxation time T2 in ms for the sample.

T2* map is obtained with a similar MATLAB code as for T2. But in this case, the first echo time is kept.

The quality of the fit can visually be assessed by plotting the corresponding exponential decay for one pixel of the image.

3.5.4 Homogeneity assessment

MRI is a non-invasive method. It allows therefore qualitative and quantitative assessment of the homogeneity of the samples investigated, as the inner structure can be reached . Homogeneity is a significant characteristic desired for the newly solid polymers manufactured. The latter are indeed expected to provide on large regions uniform values for T1, T2. For visualisation it is significant as difference of T1 or T2 within the samples will directly impact the contrast of the image.

Qualitative homogeneity assessment is performed using the 3D gradient sequences and the T1weighted and T2weighted images. They allow to directly observe by the difference of brightness the inhomogeneity of a sample. When samples are suspected to be inhomogeneous, further sagittal scans are performed to obtain a cut view of the inner part of the sample and therefore better assess it.

For quantitative homogeneity assessment five different regions of interest (ROI) are selected: in the center, at the top, at the bottom and in the right and left part of the image of the slice. The mean values for the relaxation times T1 and T2 are measured.

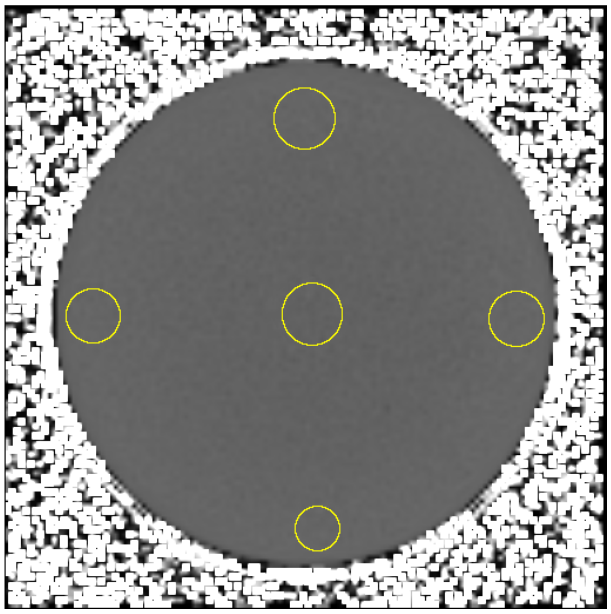

Figure 3.16: ROI selected for homogeneity assessment

The standard deviation of these values is calculated using the function "STDEV" in excel, using the "n-1" method:

$$\sqrt{\frac{\sum(x-\overline{x})^2}{(n-1)}} \tag{3.9}$$

Finally, the homogeneity of the samples is quantified as relative ratio with percentage units by dividing the latter standard deviation by the mean ROI value.

3.5.5 Error estimation

The error estimation in MR measurement is estimated in a ROI of a homogeneous region, by the standard deviation divided by square root of the sample size n:

$$\Delta x = \frac{\sigma}{\sqrt{n}} \tag{3.10}$$

The error in inhomogeneity evaluation is estimated by using the standard deviation of the mean in the different ROIs (assumed to assess inhomogenities) divided by $\sqrt{n}$.

In this thesis one significant error digits is used and printed.

4 Results

The results presented in this chapter correspond to the values obtained with the last established protocol of MR sequences for T1 : Variable flip angle, 2D Progressive saturation recovery, inversion recovery, T2 and T2*. The first section presents the results of the investigations on visibility of the 3D printed phantoms with PLA, PVA and silicone. Then, for the MR-visible materials, the results are classified according to the type of contrast liquid being used and within the sections according to the method of integration into the resin : micro-spheres or micro-capsule. T1, T2 and T2* results are reported as well as the homogeneity evaluation, when possible. Finally the last section focuses on the repeatability qualification.

4.1 3D printed phantoms

The investigation performed on the on-site materials for 3D printing aims only at qualitative assessment of the the MR visibility. As very short T2 are awaited for these solid types of materials [Berg et al., 2021], the UTE sequence has been used. Indeed, with the 3D GRE sequence no signal is obtained for the set. As put forward by figure 4.1, with the UTE sequence only the silicone type of material (in this case the heart phantom) can be visible. Remarkably, even the plastic housing of the coils produces slightly signal.

Considering these results, the cube set for MR resolution, 3D printed with PLA, is not directly visible. However, a negative contrast can be obtained by placing the phantom into a container filled with liquid. In this case the cubes have been inserted into a cup filled with silicone oil (1cSt). Choosing oil, instead of water for example, allows to avoid air bubbles being blocked within the holes of the cubes.

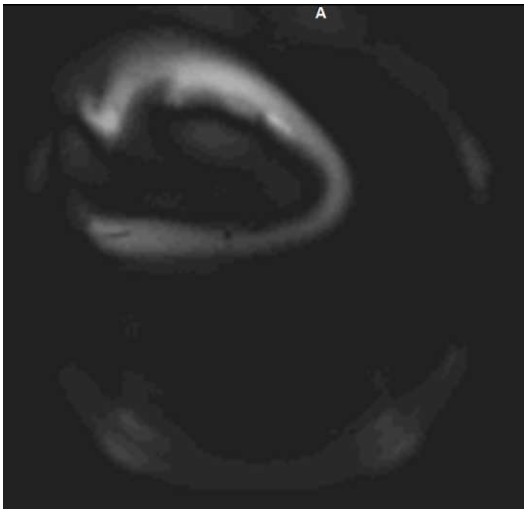

Figure 4.1: The massive walls of the artificial silicone heart can be seen in this slice selective UTE image

The 3D GRE sequence has been performed for high resolution. Figure 4.2 points out that with this MR sequence up to the third grid pattern can be correctly resolved. This corresponds to a 9 mm length cube with a period of 2 mm. If some holes don't appear, this is most probably due to a printing problem, as 1mm wall thickness is at the limit of resolution of the 3D printer.

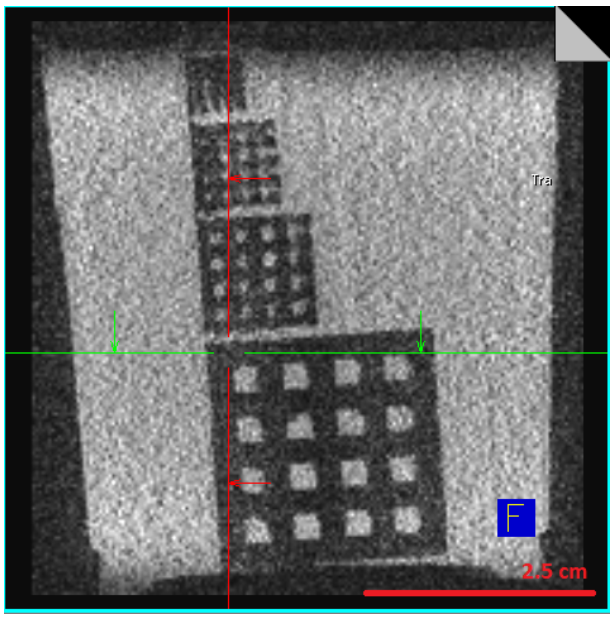

Figure 4.2: Slice image (thickness = 0.9 mm) originating from a 3D GRE sequence for investigation of 3D printing quality of a SLA printer, which is also to be used for the 3D printing of the MR visible resins.

4.2 Paraffin oil

4.2.1 Micro-spheres

The first samples received were sets of micro-spheres filled with paraffin oil. Four different sets have been produced:

Table 4.1: Sets of samples manufactured with micro-spheres filled with paraffin oil

Set	Oil [g]	Micro-spheres [g]	Resin [g]
Reference sample	30	46	130
Minus 15% oil	25.5	46	134.5
Plus 15% oil	34.5	46	125.5
Minus 25% oil	22.5	46	137.5

The investigated samples are disks of 10cm diameter and approximately 2.2cm height. Visually they all look homogeneous and opaque with a slightly yellow coloration. First, the 3D gradient sequence proves that the samples produce enough signal to be MR-visible. Figure 4.3 displays the result of the 3D GRE sequence for sample MS001, a bright disc is clearly visible. For all the other samples manufactured with micro-spheres and paraffin oil the resulting images for this 3D GRE sequence are similar.

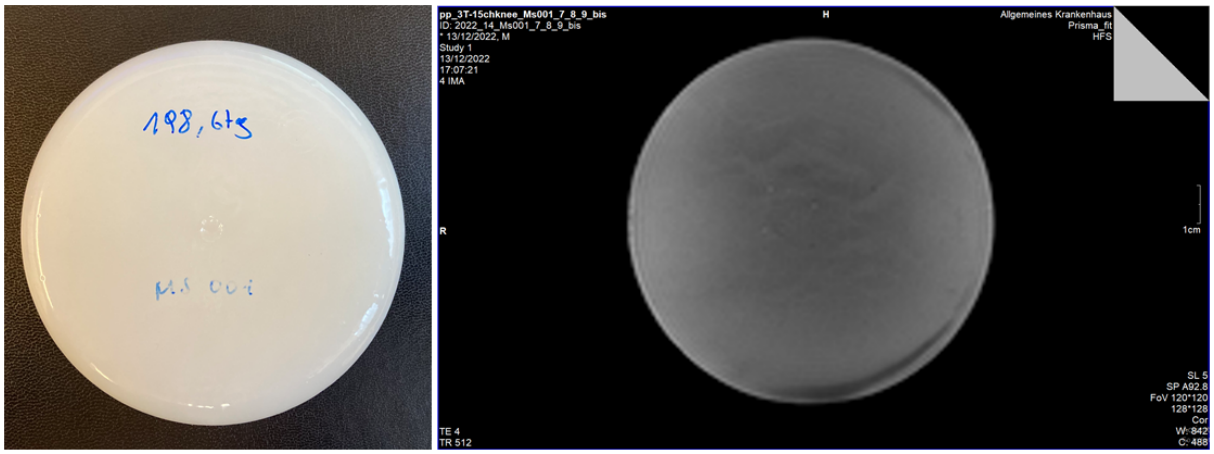

Figure 4.3: Sample MS001 and MRI image with a 3D GRE sequence

T1 and T2 assessment

T1, T2 and T2* results for the different samples are summed up on the following tables according to the type of measurement sequence :

Reference sample

Table 4.2: Reference samples

Samples	T1-VFA [ms]	T1-2D PSR [ms]	T1-IR [ms]	||	T2 [ms]	T2* [ms]
MS001	185.3 ± 14.0	179.5 ± 6.1	195.8 ± 2.9	||	94.7 ± 2.6	6.2 ± 0.7

Minus 15% oil samples

Table 4.3: T1 minus 15% oil samples

Samples	T1-VFA [ms]	T1-2D PSR [ms]	T1-IR [ms]	||	T2 [ms]	T2* [ms]
MS010	195.3 ± 16.5	187.7 ± 7.6	211.3 ± 11.3	||	103.0 ± 3.6	12.2 ± 0.6
MS011	209.8 ± 13.7	187.6 ± 8.3	206.6 ± 11.7	||	103.1 ± 3.6	11.1 ± 0.9
MS012	217.0 ± 13.7	191.3 ± 8.0	220.1 ± 11.0	||	103.1 ± 3.5	10.1 ± 0.6

Plus 15% oil samples

Table 4.4: T1 plus 15% oil samples

Samples	T1-VFA [ms]	T1-2D PSR [ms]	T1-IR [ms]	||	T2 [ms]	T2* [ms]
MS004	213.9 ± 13.5	169.5 ± 4.4	194.6 ± 3.9	||	95.3 ± 2.3	10.2 ± 1.3
MS005	185.5 ± 6.8	167.8 ± 5.4	194.6 ± 3.8	||	95.2 ± 2.3	10.4 ± 1.0
MS006	188.4 ± 4.4	169.3 ± 5.6	194.3 ± 4.1	||	95.2 ± 2.5	11.4 ± 1.1

Minus 25% oil samples

Table 4.5: T1 minus 25% oil samples

Samples	T1-VFA [ms]	T1-2D PSR [ms]	T1-IR [ms]	||	T2 [ms]	T2* [ms]
MS007	189.5 ± 10.3	167.8 ± 5.4	194.2 ± 4.8	||	95.5 ± 2.3	11.4 ± 0.8
MS008	194.7 ± 17.3	190.8 ± 12.3	193.5 ± 4.6	||	98.7 ± 3.3	6.7 ± 0.6
MS009	191.1 ± 13.8	179.2 ± 6.9	192.0 ± 4.0	||	99.0 ± 2.7	10.6 ± 1.0

The following figures are a selection for different samples of T1 and T2 maps with the corresponding fit plotted for one central pixel.

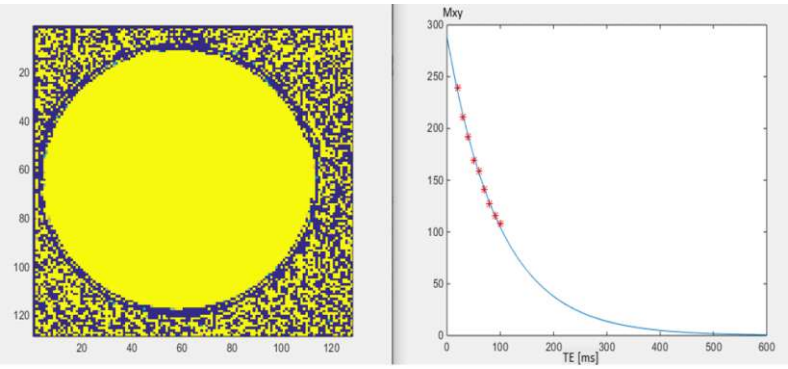

Figure 4.4: Homogeneous T2 map, T2 = 94.7 ± 2.6 ms, and corresponding fit of sample MS001

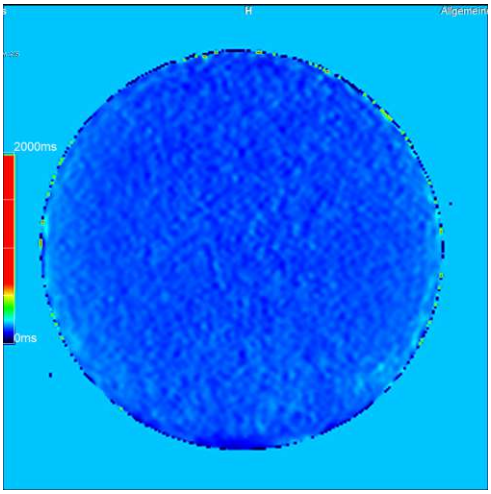

Figure 4.5: Homogeneous T1 map, T1 = 185.3 ± 14.0 ms, from the VFA sequence of sample MS001. All not fittable data points are assigned with values 240ms.

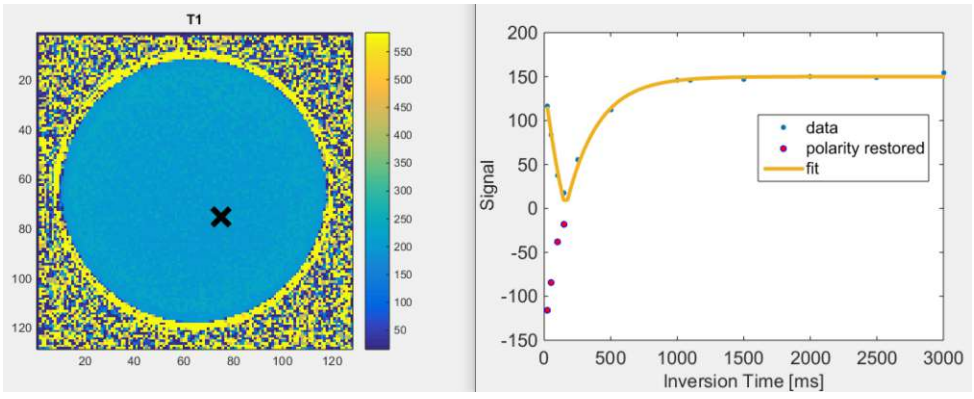

Figure 4.6: T1 map, T1 = 211.3 ± 11.3 ms, of sample MS010 and corresponding fit with the IR sequence

Homogeneity assessment

The samples are homogeneous with regard to distances of the ROI all over the sample (under 10%). There are inhomogeneities on the scale of pixel size mostly due to air bubbles and single sphere capsule agglomeration, in specific samples. In the case of sample MS009, figure 4.7 left, we clearly perceive a serie of hot spots arranged on a spiral pathway most likely related to the stirring process during manufacturing. These are not visible in the T1 and T2 maps as the voxel size is significantly larger for the mapping pulse sequences with reference to the high-resolution 3D-GRE sequence. Nevertheless, these inhomogeneities perceived in the 3D GRE sequences are reported to the manufacturer for optimization of the manufacturing process.

Table 4.6: Micro-spheres paraffin oil

Samples	T1 homogeneity (stdev)	T2 homogeneity (stdev)
MS001	2.2 %	4.5 %
MS004	1.8 %	2.8 %
MS005	1.7 %	2.8 %
MS006	1.2 %	2.4 %
MS007	1.8 %	1.9 %
MS008	1.0 %	1.8 %
MS009	1.3 %	2.3 %
MS010	2.6 %	2.5 %
MS011	3.3 %	2.5 %
MS012	1.6 %	2.8 %

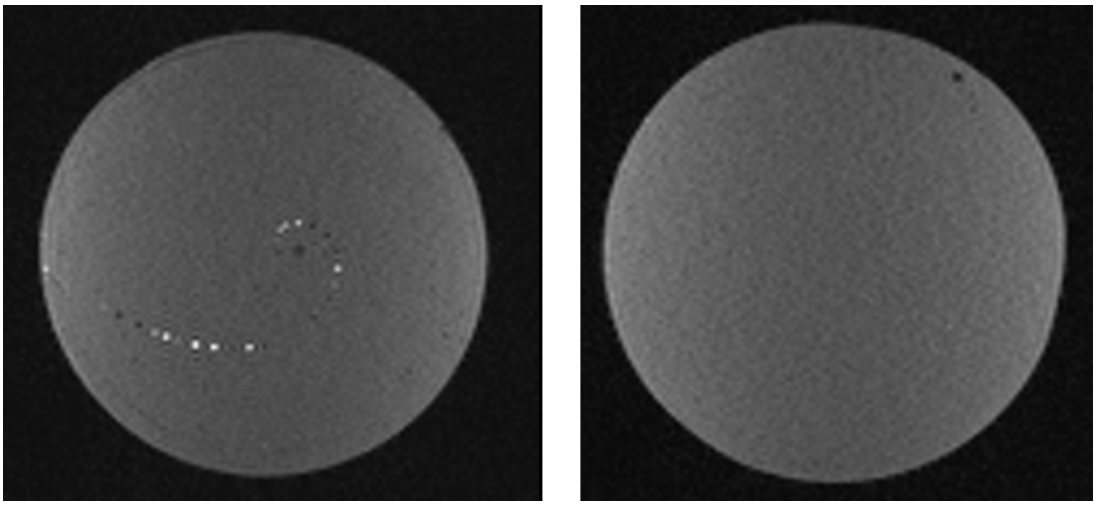

Figure 4.7: Images of samples MS009 (left) and MS008 (right) with a 3D GRE sequence

4.2.2 Micro-capsules

Samples MC003 and MC004 differ due to the size of the micro-capsules used. MC003 is composed of micro-capsules collected in a 0.5 mm sieve. MC004 is composed of smaller micro-capsules, the ones that have passed through a 0.1mm sieve. Samples MC005 and MC006 have been 3D printed using a DLP technique. Micro-capsules with paraffin oil are also MR-visible, as shown figure 4.8.

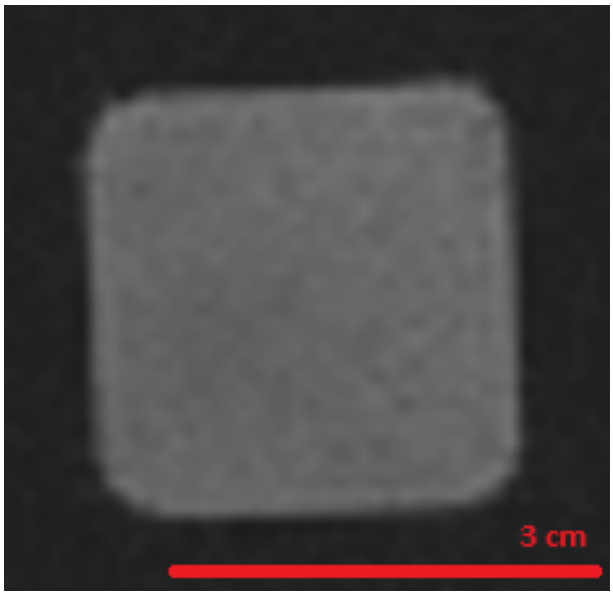

Figure 4.8: MR-scan of samples MC005 with a 3D GRE sequence

T1 and T2 assessment

Table 4.7: Micro-capsules with paraffin oil moulded samples

Samples	T1-VFA [ms]	T1-2D PSR [ms]	T1-IR [ms]	||	T2 [ms]	T2* [ms]
MC003	213.6 ± 38.0	173.4 ± 12.9	183.0 ± 5.6	||	82.7 ± 7.4	14.6 ± 0.9
MC004	209.0 ± 12.0	175.4 ± 11.1	184.4 ± 5.8	||	87.0 ± 4.9	12.2 ± 0.7

Table 4.8: Micro-capsules with paraffin oil 3D printed samples

Samples	T1-VFA [ms]	T1-2D PSR [ms]	T1-IR [ms]	||	T2 [ms]	T2* [ms]
MC005	235.6 ± 12.9	193.6 ± 13.6	195.5 ± 14.1	||	104.4 ± 6.3	6.7 ± 1.4
MC006	237.3 ± 18.5	194.7 ± 11.0	195.8 ± 16.7	||	104.8 ± 6.1	5.3 ± 1.5

Homogeneity assessment

Qualitatively, according to the regarding T1 and T2-weighted images the samples manufactured with micro-capsules and paraffin oil are homogeneous. The quantitative evaluation for T1 and T2 homogeneity is presented in the following table:

Table 4.9: T1 and T2 homogeneity results for the set of samples with micro-capsules using paraffin oil. The homogeneity is evaluated as standard deviation of the mean values in the 5 ROI distributed all over the sample as indicated in fig. 3.16

Samples	T1 homogeneity (stdev)	T2 homogeneity (stdev)
MC003	0.5 %	1.0 %
MC004	3.5 %	1.7 %
MC005	1.2 %	1.9 %
MC006	2.6 %	2.2 %

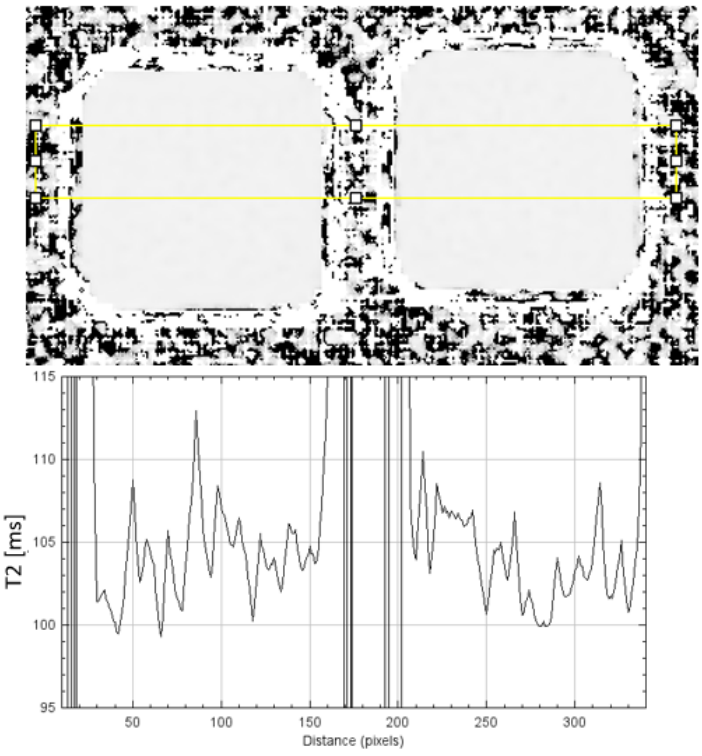

Figure 4.9: T2 map (**top**) and T2 profile (**bottom**) of samples MC005 and MC006. The maps are indicating high homogeneity and variation of maximum 13 ms in T2 values within the samples.

4.3 Silicone oil (50 cSt)

4.3.1 Micro-spheres

The preparation with micro-spheres is divided into four sets of different oil concentration. Each set is composed of three samples:

Set	Oil [g]	Micro-spheres [g]	Resin [g]
Reference samples (MS013, MS014, MS015)	30	46	130
Minus 15% oil (MS020, MS021, MS022)	25.5	46	134.5
Plus 15% oil (MS016, MS017, MS018)	34.5	46	125.5

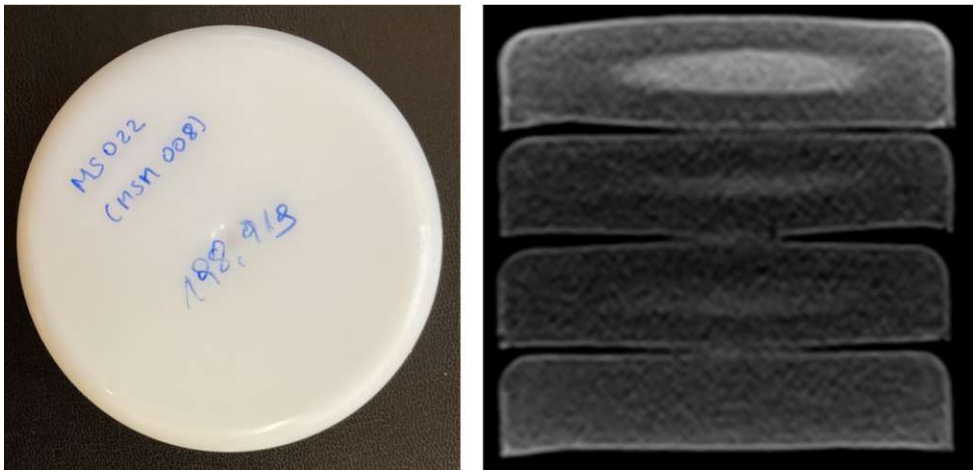

Figure 4.10: Example of a sample (MS022) manufactured with micro-spheres and 50cSt silicone oil (left). T1-weighted image of samples MS013, MS014, MS015 and MS016, respectively from bottom to top (right).

As for the paraffin oil samples, the silicone oil sample manufactured with micro-spheres are discs of 10 cm diameter and approximately 2.2 cm height. Visually they are white and opaque as shown figure 4.10. The samples produce a MR-signal. Figure 4.10 depicts a T1-weighted image in the sagittal plane of the reference set (samples MS013, MS014, MS015) and sample MS016 (+15% oil). A difference of contrast is observed within the three upper samples. This indicates that the samples are inhomogeneous.

T1 and T2 assessment

Due to reported possible inhomogeneities in the center of the samples, the measurement protocol is modified. The same MR-sequences are kept, but a variable flip angle sequence in the sagittal plane is added. The variable flip angle method allows indeed T1 mapping in a shorter and therefore reasonable time for evaluation. For the samples, where inhomogeneities have been reported, two values for T1 with the VFA sequence are measured: one for the inner central region (center), one for the outer region (periphery). For T2, on identified samples with inhomogeneities, sagittal scans are also performed. One value is reported when no inhomogeneities have been noticed in the result from the MR sequence. The T1 and T2 results for the different sequences are summed up on the following tables:

Silicone oil 50 cSt reference samples

Table 4.10: T1 values of silicone oil 50 cSt reference samples

Samples	T1-VFA [ms]	T1-2D PSR [ms]	T1-IR [ms]
MS013	1469.5 ± 145.0	954.1 ± 64.7	1305.4 ± 113.5
MS014	center: 1123.3 ± 138.8 periphery: 1419.9 ± 159.9	1002.3 ± 102.5	1351.6 ± 237.5
MS015	center: 1084.0 ± 127.2 periphery: 1386.8 ± 175.5	999.0 ± 103.2	1364.9 ± 263.7

Table 4.11: T2 and T2* values measured over a coronal slice of the samples

Samples	T2 [ms]	T2* [ms]
MS013	382.9 ± 37.5	17.1 ± 1.4
MS014	442.6 ± 68.4	31.2 ± 3.9
MS015	356.4 ± 32.9	28.1 ± 6.9

Silicone oil 50 cSt +15% oil concentration

Table 4.12: T1 values of silicone oil 50 cSt +15% oil samples

Samples	T1-VFA [ms]	T1-2D PSR [ms]	T1-IR [ms]
MS016	center: 893.7 ± 82.9 periphery : 1393.0 ± 113.2	1273.1 ± 99.0	center: 640.4 ± 29.5 periphery: 1280.0 ± 47.1
MS017	1544.5 ± 43.4	1014.9 ± 105.5	1353.4 ± 142.7
MS018	1532.4 ± 55.8	1016.3 ± 79.9	1305.7 ± 192.3

Table 4.13: T2 and T2* values of silicone oil 50 cSt +15% oil samples. No inhomogeneities are visible on the coronal T2 maps of samples MS017 and MS018.

Samples	T2 [ms]	T2* [ms]
MS016	center: 380.7 ± 27.8 periphery: 427.2 ± 44.2	18.2 ± 2.9
MS017	420.6 ± 55.3	25.4 ± 2.0
MS018	431.5 ± 71.5	26.1 ± 4.3

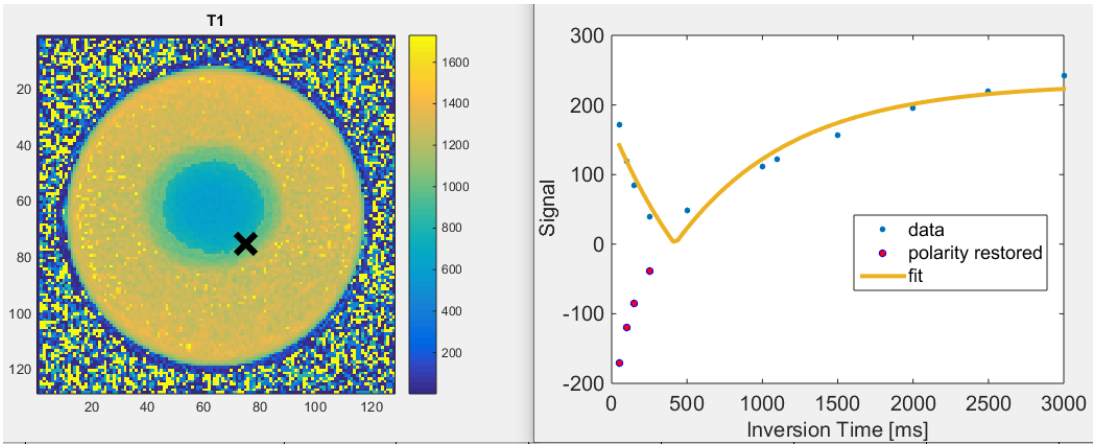

Figure 4.11: T1 map of sample MS016 with IR, and corresponding fit. The sample is clearly inhomogenous with regards to T1 values: the center part (in blue, T1 is around 640 ms) corresponds to lower T1 values while the periphery (in yellow, T1 is around 1280 ms) presents higher T1 values.

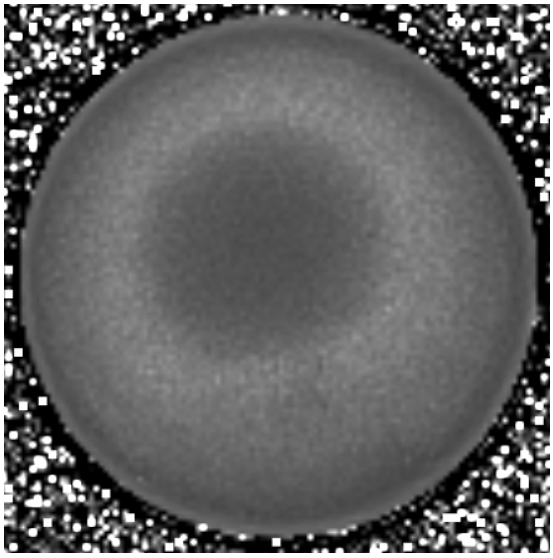

Figure 4.12: T2 map of sample MS016. The darker part in the center corresponds to lower T2 values around 380 ms.

Silicone oil 50 cSt -15% oil concentration

Table 4.14: T1 values of silicone oil 50 cSt -15% oil samples

Samples	T1-VFA [ms]	T1-2D PSR [ms]	T1-IR [ms]
MS019	center: 825.5 ± 70.3 periphery: 1502.9 ± 118.8	1000.7 ± 75.9	1363.6 ± 173.3
MS020	center: 1253.0 ± 189.6 periphery: 1520.7 ± 199.4	984.6 ± 104.1	1473.2 ± 326.3
MS021	1461.1 ± 209.7	978.0 ± 102.2	1528.2 ± 373.2

Table 4.15: T2 and T2* values of silicone oil 50 cSt -15% oil samples. No inhomogeneity is visible on the coronal T2 map of sample MS020.

Samples	T2 [ms]	T2* [ms]
MS019	center: 290.1 ± 86.0 periphery: 410.8 ± 85.9	22.2 ± 4.9
MS020	396.9 ± 61.4	24.3 ± 3.2
MS021	395.4 ± 57.4	23.5 ± 2.9

As expected all three samples from the same preparations have the same range of T1 (with respect to the sequence used), T2 and T2*. Oil concentration has no impact on these values. However, the type of oil has a main impact on the samples. In comparison to samples with paraffin oil the values for T1 and T2 have changed significantly: from approximately T1 = 200 ms and T2 = 100 ms for paraffin oil samples, to T1 = 1500 ms and T2 = 400 ms for silicone oil 50 cSt samples. The different regions observed in the T1-weighted images, corresponding to inhomogeneity within the samples, can also be found in the T1 and T2 maps (figure 4.11 and 4.12) if the slice is localised at the position of the of the inohomogeneity. The impact of this inhomogeneity is a reduced T1 and T2 in the center region.

Homogeneity assessment

Quantitative assessment of homogeneity because the samples are clearly identified as inhomogeneous. Nevertheless, for each sample, within the inhomogeneous part and outside of it (center and periphery) the T1 and T2 values are stable.

4.3.2 Micro-capsules

Only one sample with micro-capsule and silicone oil 50 cSt has been moulded. But the samples produced too little signal. The SNR is therefore too low to obtain correct T1 and T2 maps.

4.4 Silicone oil (10 cSt)

4.4.1 Micro-sphere

The preparation with micro-spheres is divided into three sets of different oil concentration. Each set is composed of three samples:

Table 4.16: Sets of samples manufactured with micro-spheres filled with silicone oil with a viscosity of $10cSt$

Set	Oil [g]	Micro-spheres [g]	Resin [g]
Reference samples (MS025, MS026, MS027)	30	46	130
Minus 15% oil (MS022, MS023, MS024)	25.5	46	134.5
Plus 15% oil (MS028, MS029, MS030)	34.5	46	125.5

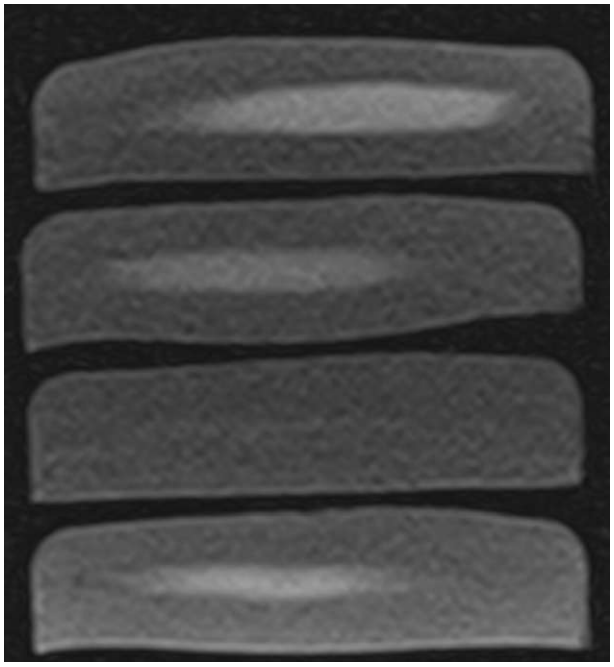

Figure 4.13: Sagittal image from samples MS025, MS026, MS027, and MS022 (bottom to top)

T1 and T2 assessment

Similarly to the samples with silicone oil 50 cSt, T1-weighted images in the sagittal plane of the reference set put forward the inhomogeneity of the samples (figure 4.13). As a consequence, the same changes to the protocol, i.e. using additional sagittal slices to evaluate T1, with the VFA sequence, and T2, are performed.

Silicone oil 10 cSt reference samples

Table 4.17: T1 values of silicone oil 10 cSt reference samples

Samples	T1-VFA [ms]	T1-2D PSR [ms]	T1-IR [ms]
MS025	center: 1738.8 ± 75.9 periphery: 1964.0 ± 96.9	1123.0 ± 99.0	1964.4 ± 117.2
MS026	1872.3 ± 105.4	1072.0 ± 111.2	2022.1 ± 199.5
MS027	1905.5 ± 204.1	1127.6 ± 125.8	2012.4 ± 231.4

Table 4.18: T2 and T2* values of silicone oil 10 cSt reference samples. No inhomogeneity is visible on the coronal T2 map of sample MS025.

Samples	T2 [ms]	T2* [ms]
MS025	621.8 ± 153.3	10.5 ± 0.9
MS026	532.2 ± 130.8	11.3 ± 1.2
MS027	608.0 ± 176.4	11.8 ± 1.1

The T1 and T2 values are increased in comparison to samples manufactured with paraffin oil and silicone oil 50cSt: T1 ranges around 2000ms and T2 ranges around 600 ms.

Silicone oil 10 cSt +15% oil concentration

Table 4.19: T1 values of silicone oil 10 cSt +15% oil concentration

Samples	T1-VFA [ms]	T1-2D PSR [ms]	T1-IR [ms]
MS028	1851.7 ± 145.3	1008.8 ± 56.7	1921.6 ± 67.4
MS029	center: 1293.1 ± 193.8 periphery: 2038.3 ± 276.3	1095.6 ± 108.9	1932.8 ± 162.6
MS030	center: 1201.0 ± 138.8 periphery: 2070.1 ± 283.2	1158.7 ± 133.6	center: 1379.3 ± 226 periphery: 1902.2 ± 176.6

Table 4.20: T2 and T2* of silicone oil 10 cSt +15% oil concentration samples.

Samples	T2 [ms]	T2* [ms]
MS028	294.0 ± 29.6	7.9 ± 1.5
MS029	center: 836.0 ± 166.0 periphery: 565.5 ± 151.1	27.0 ± 3.3
MS030	center : 928.7 ± 192.8 periphery: 649.6 ± 207.7	11.0 ± 2.5

The pattern of inhomogeneity is the same as for samples with silicone oil 50 cSt: two different T1 and T2 values in the center and in the periphery. However, for this set (MS028, MS029, MS030), T2 values are inverted in comparison to all other sets. For samples MS029 and MS030, the center has a higher T2 value than the periphery. The very low values for T2 obtained for sample MS028 seems to indicate a possible manufacturing issue for this set.

Silicone oil 10 cSt -15% oil concentration

Table 4.21: T1 values of silicone oil 10 cSt -15% oil concentration

Samples	T1-VFA [ms]	T1-2D PSR [ms]	T1-IR [ms]
MS022	center: 766.2 ± 70.4 periphery: 1929.4 ± 240.9	1268.9 ± 261.5	center: 442.8 ± 0.2 [a] periphery: 2139.7 ± 0.2[a]
MS023	center: 1006.7 ± 170.9 periphery: 2041.5 ± 301.3	1136.9 ± 129.1	center: 1551.2 ± 369.2 periphery: 1997.5 ± 193.6
MS024	center: 833.2 ± 67.5 periphery: 1904.1 ± 209.7	1200.8 ± 203.1	center: 997.5 ± 85.1 periphery: 2015.1 ± 261.8

[a] the error is relative to the fit;

Table 4.22: T2 and T2* values of silicone oil 10 cSt -15% oil concentration. No inhomogeneity is visible on the coronal T2 map of sample MS023.

Samples	T2 [ms]	T2* [ms]
MS022	center: 214.8 ± 37.1 periphery: 595.2 ± 63.2	– [b]
MS023	548.6 ± 131.7	20.3 ± 3.4
MS024	center: 457.2 ± 110.9 periphery: 557.7 ± 188.7	20.8 ± 4.4

[b] T2* was not measured before sample MS022 was cut;

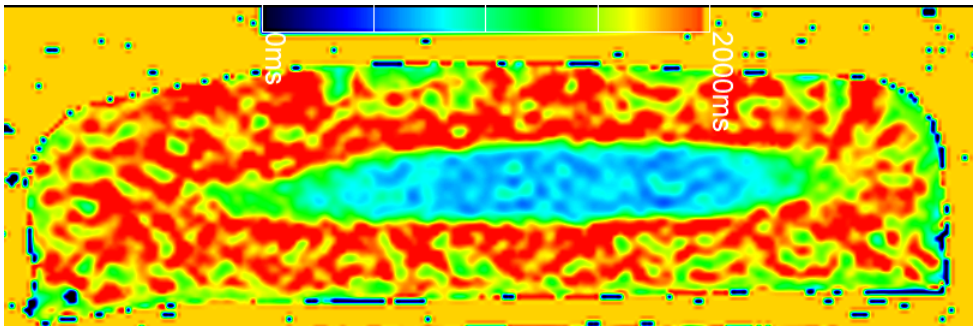

Figure 4.14: MS022 T1 map VFA

Figure 4.15: MS022 T2 map. The color scale indicates lower T2 values in bright and higher T2 values in dark, where T2 is around 595 ms. The center of sample MS022 has a T2 value around 200 ms, which is much lower than the rest of the probe.

As shown in the T1 map figure 4.14 and the T2 map figure 4.15, the center shows a reduced T1 and T2 in comparison to the periphery of the samples.

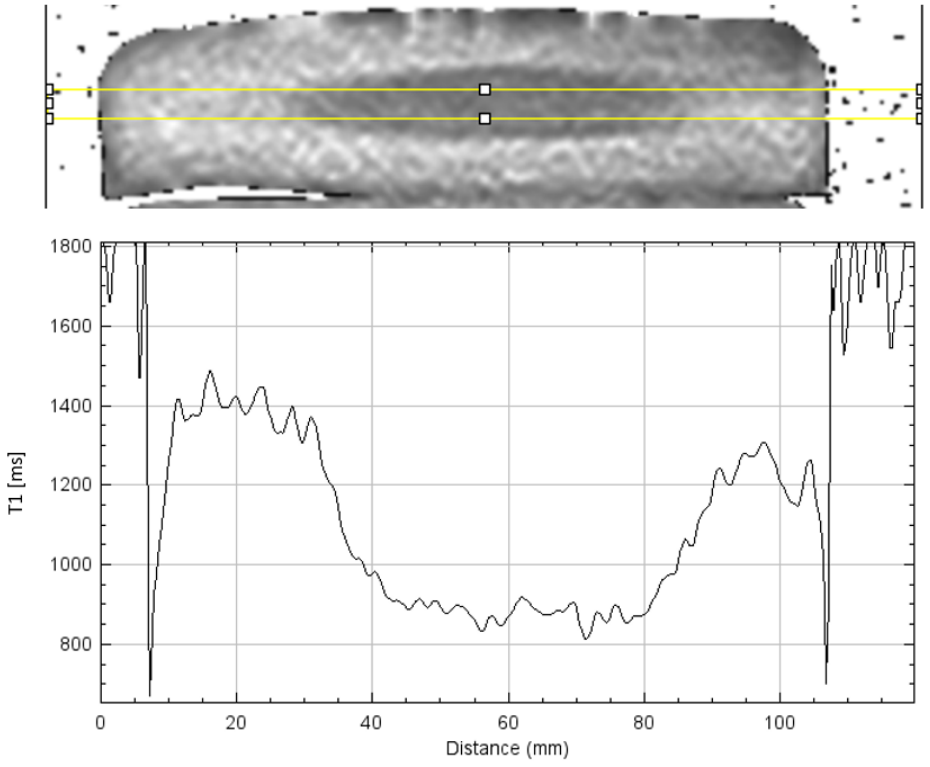

Figure 4.16: T1 map from the VFA sequence and T1 profile of sample MS016. A clear drop in the T1 value is observed in the center of the sample.

Homogeneity assessment

T1-weighted images put forward directly the inhomogeneity of most of the samples produced with Silicone oil 10 cSt. There is a clear distinction between two areas of the sample: the center and the periphery. T2 results on these two areas point out that the center has a lower T2 than the periphery: According to the BPP-theory, this suggests that the outer surrounding ring is of a less solid type of composition than the center. The size of the inhomogeneity varies between different samples: sample MS017 doesn't present this type of homogeneity, whereas for sample MS022 the central inhomogenity region is very large. However, within the two observed regions T1 and T2 are homogeneous.

Figure 4.17: Photographic image of a slice cut in the middle of sample MS022. The inhomogenity can also be observed in the optical transmission of the thin slices: the center being more transparent than the periphery.

In order to investigate the reasons for these inhomogeneities, a sagittal slice in the center of sample MS022 has been cut (figure 4.17). Sample MS022 was indeed showing a very large inhomogeneous region. This slice has been investigated with a 3D LASER microscope VK-X3000 series (Keyence, Brussels/Belgium). A surface analysis was performed in order to investigate the spatial distribution of the spheres within the sample, as any agglomeration of spheres could induce changes in T1 and T2 originating to these two different regions in the samples. However, the microscopy results, figure 4.17, indicate that there is no specific micro-sphere agglomeration in the center of the inhomogeneous samples. The micro-spheres are randomly distributed along within the samples.

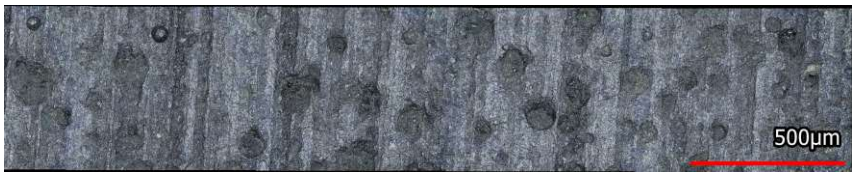

Figure 4.18: 3D LASER microscope image of the surface from the cut slice of sample MS022

4.4.2 Micro-capsule

The samples with micro-capsules and silicone oil 10 cSt have been 3D printed. They are cubes of 3.5 cm height.

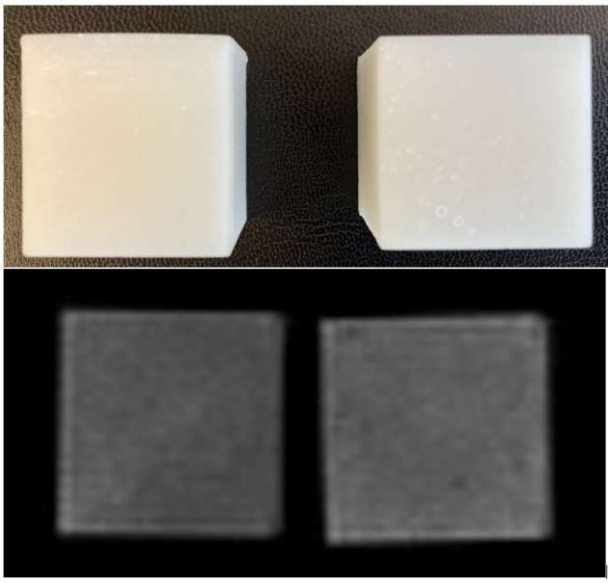

Figure 4.19: 3D printed cubes with micro-capsules and silicone oil 10 cSt

T1 and T2 assessment

In comparison to the samples manufactured with the micro-spheres and silicone oil 10 cSt, the samples with micro-capsule do not present any inhomogeneity within the samples. The T1 value over the whole sample corresponds to the T1 measured in the peripheral part of the samples with micro-spheres, in the range of about 2000 ms. Identically for T2, the values range around 600 ms as in the periphery for the micro-sphere samples.

Table 4.23: T1 values for micro-capsule samples with silicone oil 10 cSt

Samples	T1-VFA [ms]	T1-2D PSR [ms]	T1-IR [ms]
MC10cSt 1	1979.9 ± 70.4	1395.1 ± 168.6	2040.5 ± 186.5
MC10cSt 2	2074.1 ± 84.9	1472.6 ± 187.2	2093.0 ± 242.6

Table 4.24: T2 and T2* values for micro-capsule samples with silicone oil 10 cStl

Samples	T2 [ms]	T2* [ms]
MC10cSt 1	616.0 ± 55.8	18.2 ± 1.8
MC10cSt 2	581.7 ± 51.0	19.1 ± 1.8

Homogeneity assessment

Table 4.25: T1 and T2 homogeneity results for the 3D-printed samples with micro-capsules and silicone oil 10cSt

Samples	T1 homogeneity (stdev)	T2 homogeneity (stdev)
MC10cSt 1	3.0 %	4.3 %
MC10cSt 2	0.9 %	4.2 %

4.5 Water

Manufacturing samples with water has revealed to be more challenging than with oil. At this stage only one sample could be produced. However, due to the difficulty to encapsulate water in the micro-capsules, the SNR is too low. The sample can be visible by decreasing the matrix size to 64*64 (instead of 128*128), the voxel size is therefore increased and individual pixel receive an increased amount of signal (figure 4.20). The signal is nevertheless too low to perform an accurate fit for assessing T1 and T2.

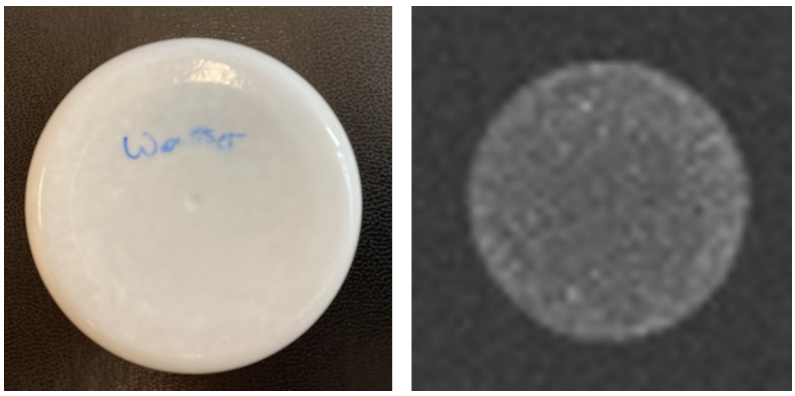

Figure 4.20: The sample composed of micro-capsules and water (left) is a moulded disc of 6.5 cm diameter and 1.5 cm height. T1-weighted image of the latter (right).

4.6 Reproducibility and time stability

In order to evaluate the stability of the samples over time, the MR measurements have been repeated two months after the first measurements. For the first received samples (micro-spheres with paraffin oil) a third repeated measurement has been performed two month after the first repetition, i.e. 4 month after first MR-measurements. As the MR sequences for T1 map have been optimized during this period, the repeatability measurements focus on the VFA sequence which was taken from the beginning.

For paraffin oil, T1 and T2 stay always within the range of error after the repeated measurements. As shown on figure 4.21 , which represents the T1 and T2 values of the set of samples MS007, MS008, MS009 (micro-spheres), no degradation has been noticed, neither a significant change of T1 over time.

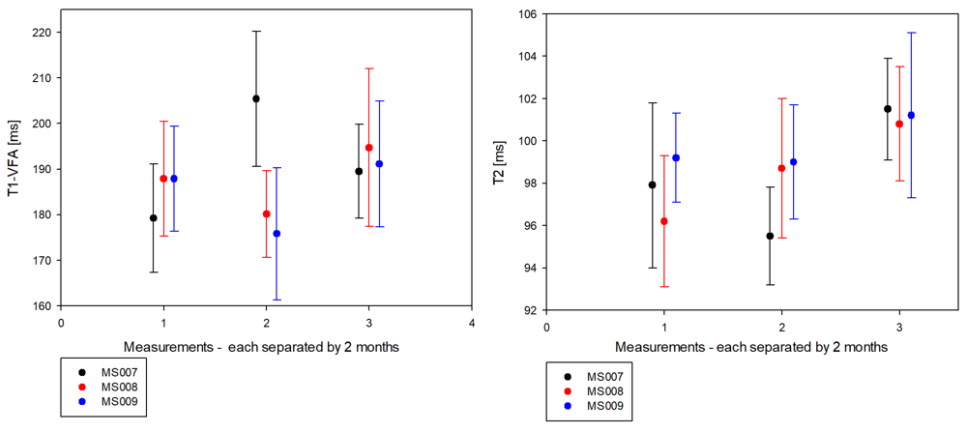

Figure 4.21: Stability on samples MS007, MS008 and MS009 with regard to T1 (left) and T2 (right) with time

T1 is varying on a larger scale for samples with micro-spheres and silicone oils.

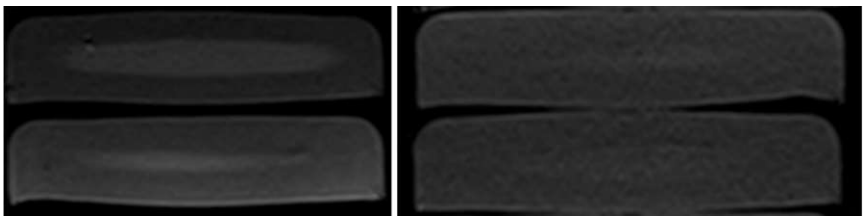

Figure 4.22: T1 weighted images of samples MS014 and MS015 after the 1st measurement (left) and after the repeated measurement (right).There is a reducing in the inhomogeneous central area.

For sample MS019, it is really relevant as the inhomogeneous part has almost completely disappeared. As depicted on the T1 map, figure 4.23, the difference in T1 in the center has disappeared and T1 is now equal to 1900ms as in the periphery. On the bottom left of the image the inhomogeneity is due to a manufacturing problem as the surface of the sample is not correctly flat. Two main hypothesis are suspected for this phenomenon : the diffusivity of the mobile oil over time or anealing processes in the resin network.

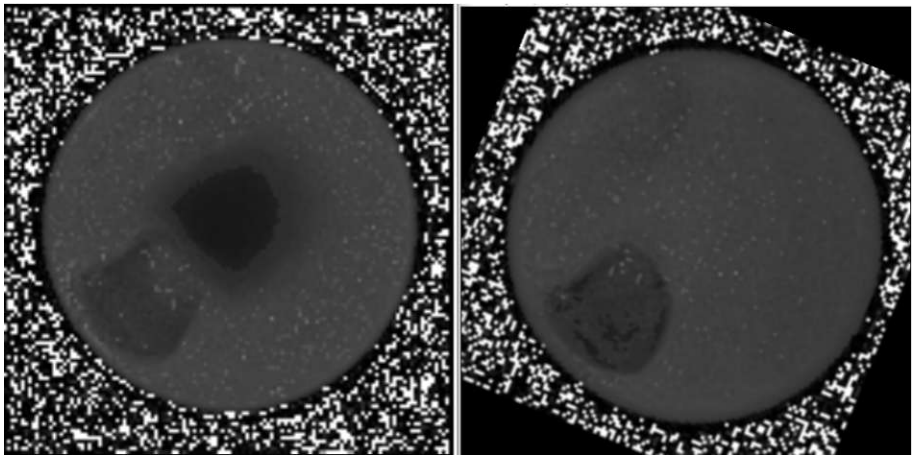

Figure 4.23: T1 maps from the IR sequence of sample MS019, after the 1st measurement (left) and after the repeated measurement (right)

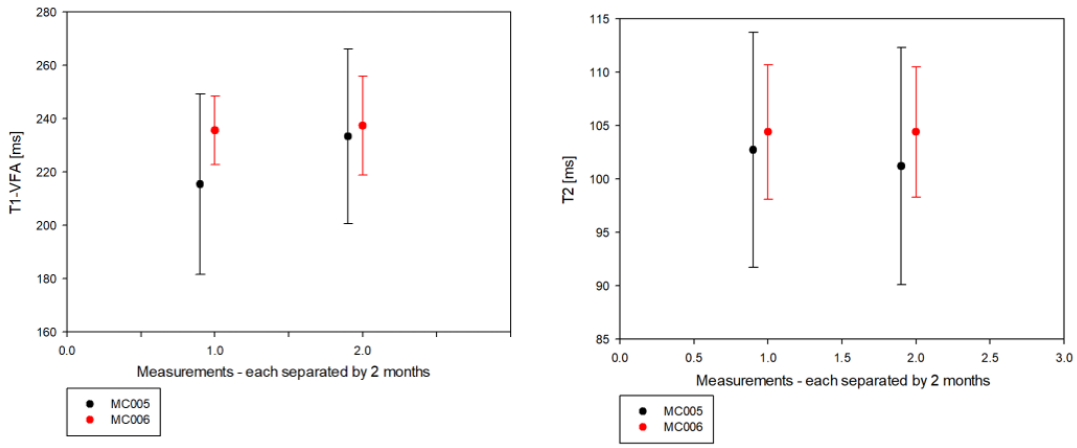

Figure 4.24: Stability on samples MC005 and MC006 with regard to T1 (left) and T2 (right) with time

For the micro-capsules, only the samples produced with paraffine oil could be investigated over 2 months. The 3D-printed samples MC005 and MC006 have been selected for their initial homogeneity. Minor changes in T1, T2 nor homogeneity, related to the measurement itself, have been noticed.

4.7 Comparison of MRI sequences for assessing T1

T1 measurements from IR, 2D PSR, and VFA are compared using the same type of phantoms: the set of micro-spheres with paraffin oil (MS007, MS008, MS009), and the set of micro-capsules with paraffin oil (MC005, MC006) are selected for comparison of the T1 values of the different pulse sequences.

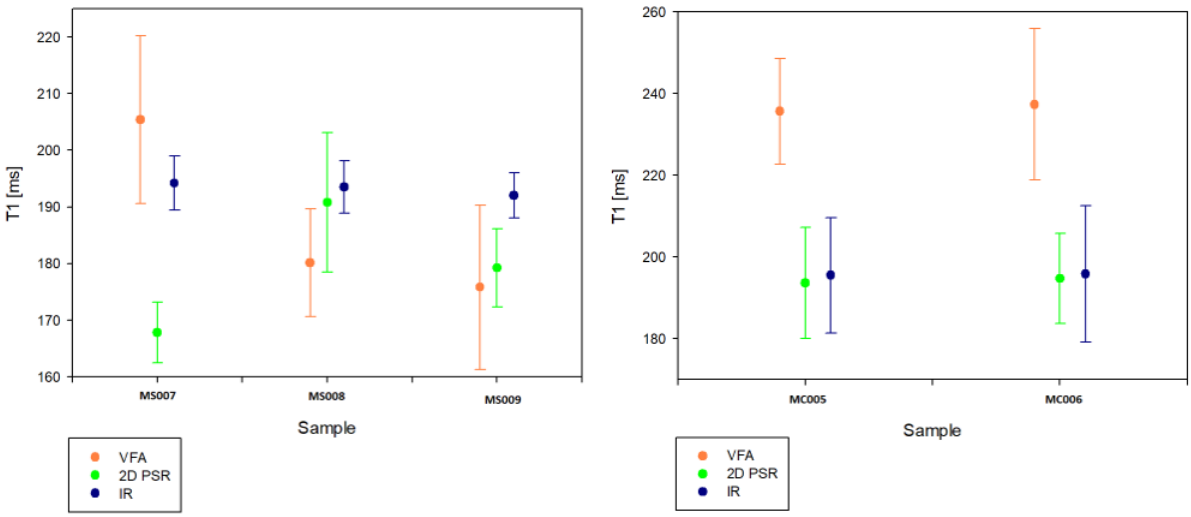

Figure 4.25: T1 values obtained from three different sequences : VFA, 2D PSR and IR for samples with micro-spheres and paraffin oil (left) and micro-capsules and paraffin oil (right)

The measured T1 values from three different pulse sequences (VFA, 2D PSR, IR) are shown in figure 4.25. For samples produced with micro-spheres (MS007, MS008, MS009), probes MS008 and MS009 delivers comparable results, with the VFA and the 2D PSR sequence underestimating the result from the IR sequence, assuming the IR results as gold standard. For sample MS007, the 2D PSR sequence highly underestimates T1, respectively T1 = 167.8 ± 5.4 ms vs T1 = 194.2 ± 4.8 ms with the IR sequence. For sample MS007 and samples manufactured with micro-capsules (MC005, MC006) the VFA sequence overestimates the results from the IR sequence. [Stikov et al., 2015] also reported that the VFA overestimates T1 but they found only slight differences in the results of the different pulse sequences (IR, VFA and Loock-Locker). It has to be noticed that the VFA sequence is very sensitive to transmit RF amplitude (B1) inhomogeneities. Performing a B1 map prior to the VFA sequence reduces inaccuracies in the resulting T1 values.

5 Discussion and Conclusion

5.1 Discussion

5.1.1 Quality assessment of MRI sequences

5.1.1.1 T1 sequences

In this thesis, three sequences for T1 mapping have been analyzed. The goal is to put forward the sequence delivering accurate results in reasonable scanning times.

Indeed, "quantitative measurement of T1 is potentially subject to significant bias and variation", as KE Keenan et al. report in their comparison of the T1 results from the IR and the VFA sequence with different MRI scanners. [Keenan et al., 2021] On repeated measurements, they underline minor variations from the IR sequence at 3T, but more bias for the VFA sequence when not combining it before to a B1 map. Moreover, they point out also a deviation of almost 10% in T1 values between scanners from different manufacturers. Differences between the VFA, the 2D PsR and the IR sequences have been observed (section "Comparison of MRI sequences for assessing T12).

Inversion recovery is the gold standard method for T1 evaluation. [Barral et al., 2010a] validated the robustness of the sequence for In Vivo studies, and [Stikov et al., 2015] "recommend to calibrate T1maps with the IR reference technique". In this master thesis, this sequence is therefore chosen as the reference for comparing the sequences for T1-map.

A significant difference between the sequences for T1 evaluation is the overall time necessary for scanning.IR requires long scanning time, which is not suited for rapid evaluation and clinical uses. In the frame of this study, IR is composed of 12 sequences of 2min43 each, in order to cover the whole recovery time of the longitudinal magnetization. The

total scanning time is therefore around 33min. For samples with longer T1, the scanning time could even increase more as the repetition time has to be increased (around five times T1). In comparison, the progressive saturation recovery sequence with 10 different repetition times last 10min. The variable flip angle sequence is even shorter: 5min. Moreover on the SYNGO software by Siemens the T1 map is directly available, whereas with the two other sequences post-processing is needed.

Therefore, for quick T1 quantification of the samples the VFA sequence proved to be the best option. However, the VFA method is very sensitive to the B1 inhomogeneities. This sequence should always be performed after a B1 map. [Lee et al., 2017]

5.1.1.2 T2 sequence

The CPMG sequence selected for T2 measurement is known for several decades, used mainly for research purposes but also for clinical applications for several decades. It is a reliable and quick method after removing the first echo in quantitative evaluation of T2. [Elster, 2023]

5.1.2 T1, T2, T2* and homogeneity assessment

Two factors are influencing T1, T2, T2* and the homogeneity of the samples :

- the contrast liquid : this parameter can be controlled by choosing the type of oil and its viscosity. The type of oil and viscosity allows to have a wide range of T1, T2 and T2* values.
- the micro-particles : micro-spheres or micro-capsule have a different impact on the homogeneity of the samples.

For each sample manufactured with paraffin oil, for both micro-spheres and micro-capsules, a T2 value around 100ms is obtained. No significant variation of T2 between the samples has been noticed, T2 values stay always in the range of error. It can be concluded that the variation of oil concentration has no impact, within variations of about +-25% oil concentration, on the T2 value. The hypothesis that the increase in oil (sphere / capsule) concentration is correlated to a higher mobility of the paraffin oil molecules and consequently T2 changes according to BPP theory is therefore not confirmed. The

result confirms an interpretation that the increase in relative oil mass contribution is resulting in an increased number of spheres without changing the mobility inside the spheres. These results underline also the stability of the material, as little variation of T2 over time is observed. This is an essential property required for phantoms, which need to be used repeatably. The small variations might be due to the complexity of MR where tiny changes in the spin environment, like temperature variations, can change the results.

For mimicking different tissues a comparison between the measured T1 and T2 values with those of tissue is relevant. Figure 5.1 offers data for the same magnetic field (T2 and T1 are dependent on the magnetic field).

Tissue	T_2—3 T [ms]		T_1—3 T [ms]	
	This study	Literature	This study	Literature
Liver	42 ± 3		812 ± 64	
Skeletal muscle	50 ± 4	32 ± 2[25]	1412 ± 13	1420 ± 38[25]
Heart	47 ± 11		1471 ± 31	
Kidney	56 ± 4		1194 ± 27	
Cartilage 0°	27 ± 3	37 ± 4[25]	1168 ± 18	~1240[25]
Cartilage 55°	43 ± 2	45 ± 67[26]	1156 ± 10	
White matter	69 ± 3	56 ± 4[27]	1084 ± 45	1110 ± 45[29]
Gray matter	99 ± 7	71 ± 10[27]	1820 ± 114	1470 ± 50[29]
Optic nerve	78 ± 5		1083 ± 39	
Spinal cord	78 ± 2		993 ± 47	
Blood	275 ± 50		1932 ± 85	~1550[30]

Figure 5.1: T1 and T2 from different tissues in [Stanisz et al., 2005].

The T2 values for some tissue (fig. 5.1) are similar to the one measured on the 3T scanner for liquid paraffin oil, T2 = 95 ± 0.5 ms, and corresponds to the one found in the literature for liquid standard mineral oil : T2 = 107.55 ± 2.77 ms in [Gach, 2019]. Regarding human tissues they are also similar to the values for gray matter : T2 = 99 ± 7 ms as shown figure 5.1. The solid samples manufactured provide therefore good opportunities for developing rigid phantoms with operator-selected T2 value for tissue mimicking. The longitudinal relaxation time T1 is around 200ms. T1 is also in the range of the values both measured on the 3T scanner and found in the literature for liquid standard mineral oil : $T1 = 205.783.35ms$ in [Gach, 2019]. However only fatty tissue (T1 about 260 ms [Stanisz et al., 2005] is close to this low value (T1 about 200 ms). Moreover there is also low difference in T1, T2 and T2* for samples moulded and samples 3D printed, when using paraffin oil.

To vary T1, T2 and T2*, silicone oil with different viscosity, 10 cSt and 50 cSt, has been used.

Samples with silicone oil present a higher T1 and T2 than with paraffin oil. Moreover, reducing the viscosity lead to higher values of T1 = 1900 ms and T2 = 600 ms (silicone oil 10 cSt) in comparison to silicone oil 50cSt, where T1 = 1500 ms and T2 = 400 ms. This is a direct consequence of the BPP-theory, as the mobility of protons is increased in a less viscous liquids. However, the use of micro-sphere or micro-capsules reduces to some extent the mobility of the oil. T2 values are then lower than the one from measured liquid silicone oil: T2 = 981.0 ± 31.3 ms for liquid silicone oil 10cSt vs T2 = 616.0 ± 55.8 ms for a sample with micro-capsules and silicone oil 10cSt. This could also result from the inherent magnetic susceptibility difference between the spheres, the resin and the MR-visible liquid, which leads to spatial magnetic field fluctuation. Increased values for T1 and T2 are interesting with regards to producing phantoms for mimicking tissues. High T1, around 2000ms, for samples with micro-capsules and silicone oil 10cSt are comparable to the T1 measured by [Stanisz et al., 2005] for blood (figure 5.1).

Regarding the homogeneity of the samples manufactured with silicone oil, inhomogeneities have been found in the samples with micro-spheres but not in the samples with micro-capsules. The microscopy investigation of the slice from a sample manufactured with micro-spheres and silicone oil 10cSt proved that the observed inhomogeneity in the sample is not linked to an agglomeration of the spheres. Indeed as shown by figure 4.18 the spheres are randomly distributed in the sample. Two hypothesis are then made to explain the observed inhomogeneity in samples with silicone oil 10cSt and 50cSt. It can be related to the hardening process with UV light, or it is related to the polymer network density. During the UV irradiation more dense networks could have moved to the periphery creating a difference with lower density network in the center. Repeated measurement indicates that the inhomogeneity within the sample tends to decrease, which might be related to the diffusion of the oil over time or annealing network changes. On the contrary samples manufactured with micro-capsules and silicone oil are homogeneous.

The micro-capsules proved to deliver the most reproducible results and perspectives for the development of practical applications as they can be used in 3D printing process.

5.2 Conclusion and outlook

The current project proved that the presented patented manufacturing technique is able to deliver solid materials that are visible through MRI. These materials can be quantitatively assessed by means of MR parameters T1, T2 and T2*. For the first time, we demonstrated that by adjusting the types of add-ons we could create homogeneous samples with a wide range of T1, around 200ms, 1500ms and 2000ms, and T2 values, around 100ms, 500ms and 600ms. The material is stiff and stable over time. The samples proved also to be successfully 3D-printed while keeping their MR-visible property. This is a significant step as it offers the possibility to use CAD designing for resin based samples

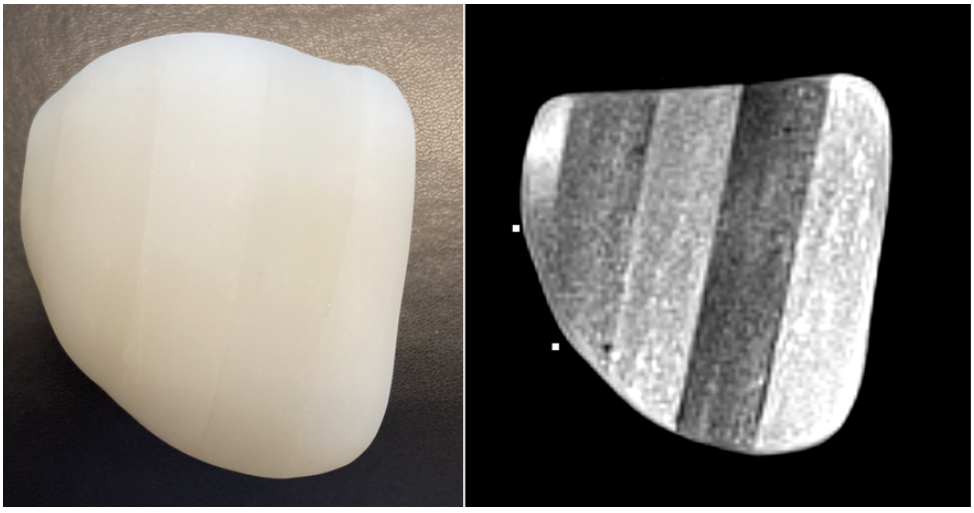

Figure 5.2: 1:1 scaled heart phantom (left), manufactured with four 3D printed slices with micro-capsules and paraffin oil. Spin density map of the heart phantom (right), the differences between the slices are clearly visible due to difference of brightness. This indicates differences in capsule concentration and agglomeration during the production process.

The manufacturing process is the main challenge for improving the quality of the materials. One major issue with the produced samples is the intensity of the MR-signal. The latter is determined by the concentration of micro-capsules/micro-spheres within the samples. The lower the number of micro-capsules/micro-spheres the lower is the spin density in the samples and therefore the intensity. As shown in figure 5.2, the heart composed of four slices, glued together, presents differences in contrast, even though the slices were produced within the same batch of micro-capsules. The size and the distribution of the micro-capsules during 3D printing are parameters that are difficult to control at present. Moreover, regarding MRI investigations, measurements performed on a higher magnetic

field strength $B_0 = 7$ T (oral report A. Berg) were not conclusive, due to low and inhomogeneous signal. Even though, the T1 and T2 values are now sufficiently high, no signal was measured. One reason could be a very short T2* decay in this type of scanner (oral report A. Berg). T2* is very sensible to magnetic susceptibilities and therefore inhomogeneities within the samples. Susceptibility differences might increase non-linearly with magnetic strength, reducing significantly T2*. Further investigations have to be performed.

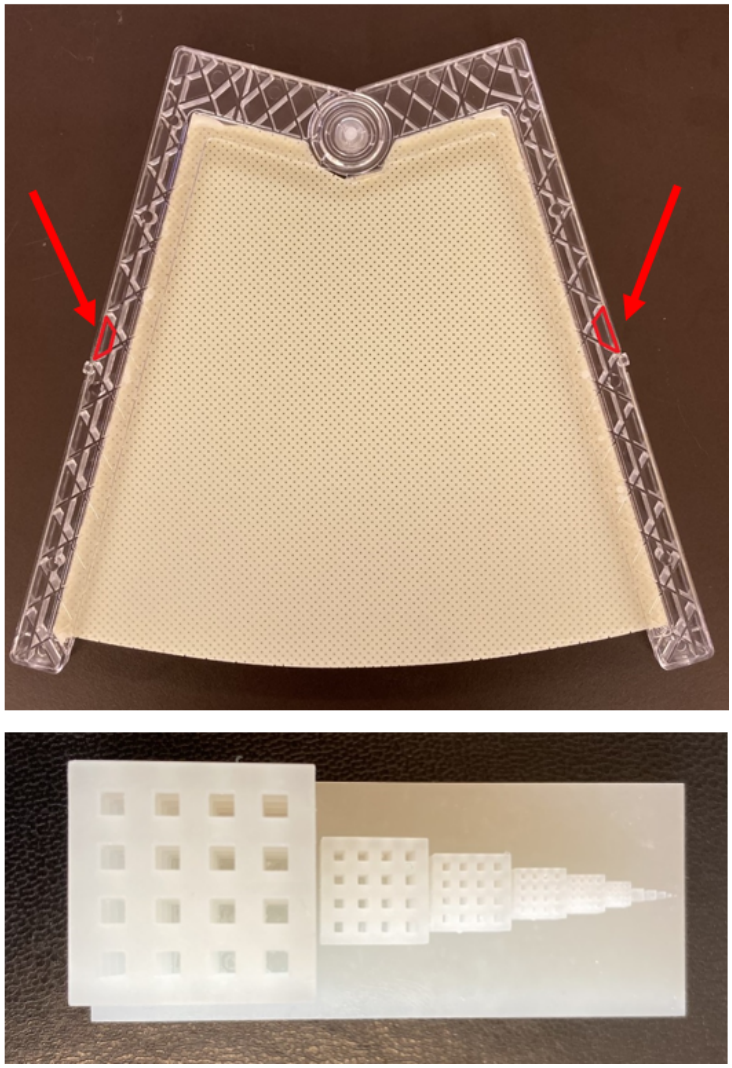

Figure 5.3: Examples of applications of the MR-visible solid resin : MR-visible inserts (underlined in red) for patient head position localisation in radiation therapy (top) ; 3D resolution cubes (bottom)

Future developments of the materials will focus on improving the manufacturing process to make it more reproducible. Increasing the concentration of micro-capsules/microspheres and varying the type of liquids used for production, like mixtures with Gd, are

the significant next step in the production process investigations. A wider selected range of T1 and T2 would give outlooks for applications. For medical applications the choice of bio-compatible materials for, especially the type of resin, will be also necessary. Finally, cooperation with private companies would allow a production on a larger scale.

Three types of direct practical applications have been manufactures by Markus Ortner and MR-measured within this master thesis, as shown figure 5.2 and figure 5.3 :

- Phantom for mimicking tissue : a model of a heart has been 3D printed.
- Resolution phantom for MR : cube set with a grid pattern. The principle design of the resolution phantom has been proposed and implemented by A. Berg [Berg, 2015]. The STL-files have been adapted for larger size within this master thesis using an available CAD design program.
- Localisation part for MR-guided radiation therapy.

In this three fields of application and beyond, this new MR-visible solid resin offers already new outlooks and prospects for research and development.

Bibliography

[Barral et al., 2010a] Barral, J. K., Gudmundson, E., Stikov, N., Etezadi-Amoli, M., Stoica, P., and Nishimura, D. G. (2010a). A robust methodology for in vivo T1 mapping. *Magnetic resonance in medicine*, 64(4):1057–1067.

[Barral et al., 2010b] Barral, J. K., Gudmundson, E., Stikov, N., Etezadi-Amoli, M., Stoica, P., and Nishimura, D. G. (2010b). A robust methodology for in vivo T1 mapping. *Magn. Reson. Med.*, 64(4):1057–1067.

[Baudrexel et al., 2018] Baudrexel, S., Nöth, U., Schüre, J.-R., and Deichmann, R. (2018). T1 mapping with the variable flip angle technique: a simple correction for insufficient spoiling of transverse magnetization. *Magnetic resonance in medicine*, 79(6):3082–3092.

[Berg, 2015] Berg, A. (2015). 2-3-Dimensional -Structures for Magnetic Resonance Microscopy, KNMF project Proposal-ID: 2015-013-006488 (2015).

[Berg et al., 2021] Berg, A. G., Hatamikia, S., Valladares, A., Ptacek, W., Kronreif, G., and Lorenz, A. (2021). High-field MRI of Polymer/Silicone material for body compartment phantoms and interventional devices: Visibilty with Standard GRE MR protocols, UTE-imaging and quantitative T1/T2 determination. *Proc. Joint Conference of the ÖGMP, DGMP SGSMP Dreiländertagung Medizinische Physik 2021,eP21; 159-160 19.-22.09.21 DIGITAL https://www.medical-physics2021.com/index.php?id=3315 2021.*

[Birkbeck, 2023] Birkbeck, M. (2023). Parametric Mapping Scripts for MRI data. `https://www.mathworks.com/matlabcentral/fileexchange/64579-parametric-mapping-scripts-for-mri-data`. Accessed: (2023-04).

[Bloch, 1946] Bloch, F. (1946). Nuclear induction. *Physical review*, 70(7-8):460.

[Bloembergen et al., 1948] Bloembergen, N., Purcell, E. M., and Pound, R. V. (1948). Relaxation effects in nuclear magnetic resonance absorption. *Physical review*, 73(7):679.

[Bogaert et al., 2019] Bogaert, S. M., Vandemaele, P. M., and Pullens, P. P. (2019). GIfMI MRI user manual SIEMENS PRISMA. `http://gifmi.ugent.be/drupal/system/files/documents/GIfMI_MRI%20user%20manual_BASIC_SiemensPrisma_EN.pdf`. Accessed: (2023-01).

[Boudreau, 2023] Boudreau, M. (2023). Interactive T1 mapping book. `https://qmrlab.org/jekyll/2023/01/16/T1_book.html`. Accessed: (2023-04).

[Boudreau et al., 2017] Boudreau, M., Tardif, C. L., Stikov, N., Sled, J. G., Lee, W., and Pike, G. B. (2017). B1 mapping for bias-correction in quantitative T1 imaging of the brain at 3T using standard pulse sequences. *Journal of magnetic resonance imaging*, 46(6):1673–1682.

[Carr and Purcell, 1954] Carr, H. Y. and Purcell, E. M. (1954). Effects of diffusion on free precession in nuclear magnetic resonance experiments. *Physical review*, 94(3):630.

[Czerny, 2022] Czerny, R. (2022). *Flexible Coil Arrays for Magnetic Resonance Imaging–Performance Comparison of Coaxial Transmission Line Resonators and Stranded Wire Elements*. PhD thesis, Technische Universität Wien.

[Demtröder, 2016] Demtröder, W. (2016). *Experimentalphysik 3: Atome, Moleküle und Festkörper, Edition 5*. Springer-Verlag.

[Elster, 2023] Elster, A. D. (2023). Questions and answers in MRI, "Courtesy of Allen D. Elster, MRIquestions.com". `https://mriquestions.com`. Accessed: (2023-01).

[Ernst and Anderson, 1966] Ernst, R. R. and Anderson, W. A. (1966). Application of fourier transform spectroscopy to magnetic resonance. *Review of Scientific Instruments*, 37(1):93–102.

[Fram et al., 1987] Fram, E. K., Herfkens, R. J., Johnson, G. A., Glover, G. H., Karis, J. P., Shimakawa, A., Perkins, T. G., and Pelc, N. J. (1987). Rapid calculation of T1 using variable flip angle gradient refocused imaging. *Magnetic Resonance Imaging*, 5(3):201–208.

[Gach, 2019] Gach, H. M. (2019). T1 and T2 and complex permittivities of mineral oil, silicone oil, and glycerol at 0.35, 1.5, and 3 T. *Medical physics*, 46(4):1785–1792.

[Hahn, 1950] Hahn, E. L. (1950). Spin echoes. *Physical review*, 80(4):580.

[Holmes and Bydder, 2005] Holmes, J. E. and Bydder, G. M. (2005). MR imaging with ultrashort TE (UTE) pulse sequences: Basic principles. *Radiography*, 11(3):163–174.

[Jo et al., 2019] Jo, Y., Kim, J., Park, C. H., Lee, J. W., Hur, J. H., Yang, D. H., Lee, B. Y., Im, D. J., Hong, S. J., Kim, E. Y., et al. (2019). Guideline for cardiovascular magnetic resonance imaging from the korean society of cardiovascular imaging-part 1: standardized protocol. *Korean J Radiol*, 20(9):1313.

[Karakuzu et al., 2020] Karakuzu, A., Boudreau, M., Duval, T., Boshkovski, T., Leppert, I., Cabana, J.-F., Gagnon, I., Beliveau, P., Pike, G., Cohen-Adad, J., and Stikov, N. (2020). qMRLab: Quantitative MRI analysis, under one umbrella. *J. Open Source Softw.*, 5(53):2343.

[Keenan et al., 2021] Keenan, K. E., Gimbutas, Z., Dienstfrey, A., Stupic, K. F., Boss, M. A., Russek, S. E., Chenevert, T. L., Prasad, P., Guo, J., Reddick, W. E., et al. (2021). Multi-site, multi-platform comparison of MRI T1 measurement using the system phantom. *PloS one*, 16(6):e0252966.

[Kingsley, 1999] Kingsley, P. B. (1999). Signal intensities and T1 calculations in multiple-echo sequences with imperfect pulses. *Concepts in Magnetic Resonance: An Educational Journal*, 11(1):29–49.

[Lee et al., 2017] Lee, Y., Callaghan, M. F., and Nagy, Z. (2017). Analysis of the precision of variable flip angle T1 mapping with emphasis on the noise propagated from rf transmit field maps. *Frontiers in neuroscience*, 11:106.

[Mansfield, 1982] Mansfield, P. (1982). *Nmr imaging in biomedicine: Supplement 2 advances in magnetic resonance*, volume 2. Elsevier.

[Milford et al., 2015] Milford, D., Rosbach, N., Bendszus, M., and Heiland, S. (2015). Mono-exponential fitting in t2-relaxometry: relevance of offset and first echo. *PloS one*, 10(12):e0145255.

[Oystaeyen, 2018] Oystaeyen, B. V. (2018). Physique pour la médecine. https://www.phys4med.be/irm. Accessed: (2023-04).

[Rai et al., 2020] Rai, R., Holloway, L. C., Brink, C., Field, M., Christiansen, R. L., Sun, Y., Barton, M. B., and Liney, G. P. (2020). Multicenter evaluation of MRI-based radiomic features: A phantom study. *Medical physics*, 47(7):3054–3063.

[Rausch et al., 2022] Rausch, I., Valladares, A., Unger, E., Berg, A., and Rosenbüchler, P. (2022). Method for producing a light-curable resin composition (ep 3 974 903 al).

[Reiser et al., 2007] Reiser, M. F., Semmler, W., and Hricak, H. (2007). *Magnetic resonance tomography*. Springer Science & Business Media.

[Robinson, 2023] Robinson, S. (2023). Siemens DICOM sort and convert to NIfTI. https://www.mathworks.com/matlabcentral/fileexchange/22508-siemens-dicom-sort-and-convert-to-nifti. Accessed: (2023-04).

[Robson et al., 2003] Robson, M. D., Gatehouse, P. D., Bydder, M., and Bydder, G. M. (2003). Magnetic resonance: an introduction to ultrashort TE (UTE) imaging. *Journal of computer assisted tomography*, 27(6):825–846.

[Stanisz et al., 2005] Stanisz, G. J., Odrobina, E. E., Pun, J., Escaravage, M., Graham, S. J., Bronskill, M. J., and Henkelman, R. M. (2005). T1, T2 relaxation and magnetization transfer in tissue at 3T. *Magnetic Resonance in Medicine: An Official Journal of the International Society for Magnetic Resonance in Medicine*, 54(3):507–512.

[Steen et al., 1994] Steen, R. G., Gronemeyer, S. A., Kingsley, P. B., Reddick, W. E., Langston, J. S., and Taylor, J. S. (1994). Precise and accurate measurement of proton T1 in human brain in vivo: validation and preliminary clinical application. *Journal of Magnetic Resonance Imaging*, 4(5):681–691.

[Stikov et al., 2015] Stikov, N., Boudreau, M., Levesque, I. R., Tardif, C. L., Barral, J. K., and Pike, G. B. (2015). On the accuracy of T1 mapping: searching for common ground. *Magnetic resonance in medicine*, 73(2):514–522.

[Systems, 1990] Systems, P. M. (1990). *Basic Principles of MR Imaging*. Philips Medical Systems, Philips Medical Systems Nederland.

[Talalwa et al., 2019] Talalwa, L., Gordji-Nejad, A., Natour, G., Drzezga, A., Bauer, A., and Beer, S. (2019). Evaluation of 3D printable rubber-elastomeric polymer as phantom material for Hybrid PET/MRI. In *2019 IEEE Nuclear Science Symposium and Medical Imaging Conference (NSS/MIC)*, pages 1–3. IEEE.

Appendix

Source files

All the source files are available on the private ftp account sftp://sftp1.meduniwien.ac.at:

1. Evaluation file containing the measurement data (T1, T2, T2*): Excel file "Probendaten und Terminplan_09_08_2023"
2. Source data containing the DICOM data: File "MD"

MATLAB script for T1 mapping

```
%%
clear all
clc
tic

%% Loading the data

dname = uigetdir;
dimages = strcat(dname,'/*.IMA');
directory = dir (dimages);
addpath(dname)
files = {directory.name};

Image1 = dicomread(files{1});
[x,y] = size(Image1(:,:,1)); % or [x,y,~] = size(Image1)

% Input the number of slices and the repetition times
```

```
prompt = 'Number of slices :';
Nbslices = input(prompt);
prompt = 'Repetition Times ([mintime,...,maxtime] :';
reptimes=input(prompt);

%% Creating stacks of slices with their repetition time

Slices=cell(1,Nbslices);
rep=cell(1,length(reptimes));
start=1; %Not taking into account the first echo for the
   slices to suppress the first echo
for k=1:Nbslices
    for j=1:length(reptimes)
        rep(j)=files(start);
        if start+Nbslices < length(files)
            start=start+Nbslices;
        end
    end
    Slices{k}=rep;
    if start < length(files)
        start=(start-((length(reptimes)-1)*(Nbslices)))+1;
    end
end

% Read in dicomread files and concatenate them into a matrix
   gives a (M x N x nRepetition x nSlice) Matrix
tr_image = zeros(x,y,length(reptimes),size(Image1,3));

for i=1:length(Slices)
    S=Slices{i};
    for n=1:length(S)
        imrep=S{n};
        tr_image(:,:,n,i) = dicomread(imrep);
    end
end
```

```
51
52
53  %% Analysis of slices
54
55  prompt = 'Taking offset ? (Answer by yes or no) :';
56  offset = input(prompt);
57  prompt = 'Slice selection ([first_slice , last_slice]) :';
58  sliceselec = input(prompt);
59
60  C=cell(1,sliceselec(2));
61
62  for k = sliceselec(1):sliceselec(2)%size(tr_image(:,:,:,:),4)
63
64      Img = tr_image(:,:,:,k);
65      [x,y,nInversion] = size(Img); % dimension of the Image
66      ImageT1=zeros(x,y);
67      C{k}=cell(1,x*y);
68      c=C{k};
69      ymat = reshape(Img,[],nInversion);
70      Ymat=zeros(size(ymat));
71      st=size(ymat,2);
72      for p=1:size(ymat,2)
73          Ymat(:,p)=ymat(:,st);
74          st=st-1;
75      end
76
77
78      % xdata is a vector which contains the time for each
           pixel element
79      % in Y
80      Xdata = reptimes';
81
82      % Selection of the function to fit with or without offset
83      if strcmp(offset,'yes') == 1
84          fun = @(x,xdata) x(1)*(1-exp(-xdata/x(2)))+x(3);
```

```
85      else
86          fun = @(x,xdata) x(1)*(1-exp(-xdata/x(2)));
87      end
88
89      % Loop over each pixel
90      parfor i = 1:x*y
91          if sum(ymat(i,:))~=0
92              Ydata=Ymat(i,:)';
93              %g = fittype('a*(1-exp(-x/b))+c');
94              opts = optimset('Display','off');
95              f=lsqcurvefit(fun,[200,1500,10],Xdata,Ydata,[-Inf
                    ,-Inf,-Inf],[+Inf,+Inf,+Inf],opts); %20
96
97              %f = fit(Xdata,Ydata,g,'Lower',[40,170,10],'Upper
                    ',[2000 2000 100],'StartPoint',[200,200,20]);
98              if f(2)~=0
99                  T1=f(2);
100                 if strcmp(offset,'yes') == 1
101                     h=@(x) f(1)*(1-exp(-x/f(2)))+f(3);
102                 else
103                     h=@(x) f(1)*(1-exp(-x/f(2)));
104                 end
105                 c{i}=h;
106                 ImageT1(i)=T1;
107             end
108         end
109
110
111
112     end
113     C{k}=c;
114     IM16 = uint16(ImageT1);
115     filename = ['ImageT1_2DPSR_with_offset_MS016', num2str(k)
            , '_','.tiff'];
116     imwrite(IM16,parula,filename);
```

```
end
toc


%% Plotting the fit
figure();
image(ImageT1);
prompt = 'Plot fit ? (Answer by pixel position [X,Y] or no) :
    ';
pix = input(prompt);

while strcmp(pix,'no')==0
    figure();
    plot(reptimes,Ymat(128*(pix(1)-1)+pix(2),:),'*r');
    hold on;
    fplot(c{128*(pix(1)-1)+pix(2)},[0,max(reptimes)+100]);
    prompt = 'Plot fit ? (Answer by pixelnumber or no) :';
    pix = input(prompt);
end
```

MATLAB script for T2 mapping

```
% Original script from matt birkbeck (2022). Parametric
    Mapping Scripts for MRI data (https://www.mathworks.com/
    matlabcentral/fileexchange/64579-parametric-mapping-
    scripts-for-mri-data), MATLAB Central File Exchange.
    Retrieved November 9, 2022.
clear all
clc

tic

%% Loading the data

dname = uigetdir;
```

```
dimages = strcat(dname,'/*.IMA');
directory = dir (dimages);
addpath(dname)
files = {directory.name};

%% User selection of the parameters

prompt = 'Number of slices :';
Nbslices = input(prompt);
prompt = 'Number of echoes :';
Nbechoes = input(prompt);
prompt = 'Selection of first echo ? (yes or no) :';
selecfirstecho = input(prompt);
prompt = 'Echo Times :';
echotimes=input(prompt);


%% Creating stacks of slices with their echoes times without
   the first echo

Slices=cell(1,Nbslices);
if strcmp(selecfirstecho,'no') == 1
    echo=cell(1,Nbechoes-1);
else
    echo=cell(1,Nbechoes);
end

if strcmp(selecfirstecho,'no') == 1
    start=Nbslices+1; %Not taking into account the first echo
        for the slices to suppress the first echo
else
    start=1;
end

for k=1:Nbslices
```

```
    for j=1:(Nbechoes-1)
        echo(j)=files(start);
        if start+Nbslices < length(files)
            start=start+Nbslices;
        end
    end
    Slices{k}=echo;
    if start < length(files)
        if strcmp(selecfirstecho,'no') == 1
            start=(start-((Nbechoes-1)*(Nbslices)))+Nbslices
               +1; %Not taking into account the first echo
                for the slices to suppress the first echo
        else
            (start-((Nbechoes-1)*(Nbslices)))+Nbslices+1;
        end

    end
end

%% Read dicom files and concatenate them into a (M x N x
   nEchoes x nSlices) Matrix called te_image

Image1 = dicomread(files{1});
[x,y] = size(Image1(:,:,1));
te_image = zeros(x,y,(Nbechoes-1),Nbslices);

for i=1:length(Slices)
    S=Slices{i};
    for n=1:length(S)
        imecho=S{n};
        te_image(:,:,n,i) = dicomread(imecho);
    end
end

%% Analysis of slices
```

```
75 prompt = 'Slice selection ([first_slice , last_slice]) :';
76 sliceselec = input(prompt);
77 C=cell(1,sliceselec(2));
78
79 for k = sliceselec(1):sliceselec(2)%size(te_image(:,:,:,:),4)
80
81     Img = te_image(:,:,:,k);
82     [x,y,nEcho] = size(Img); % dimension of the Image
83     ImageT2=zeros(x,y);
84     C{k}=cell(1,x*y);
85     c=C{k};
86
87     % to get a 1D array representing our Img matrix the Img
          matrix is
88     % re-written to a 1D vector Ydata - this represents our (
          x*y)
89     % seperate problems with nEchos data points (nEchos) in
          each problem.
90     ymat = reshape(Img,[],nEcho);
91     Xdata=echotimes';
92
93     %fun = @(x,xdata) x(1)*(exp(-xdata/x(2)));
94
95     for i=1:x*y
96         if sum(ymat(i,:))~=0
97             Ydata=ymat(i,:)';
98             %f=lsqcurvefit(fun,[200,90],Xdata,Ydata);
99             f=fit(Xdata,Ydata,'exp1');
100            if f.b~=0
101                T2=-(1/f.b);
102                ImageT2(i)=T2;
103                h=@(x) (f.a)*(exp(-x/T2));
104                c{i}=h;
105            end
106        end
```

```
    end

    %Display the image
    %figure()
    %image(ImageT2);

    %Image in .bmp format
    %filename1 = ['ImageT2w_MC003_004_slice', num2str(k), '_
       ','.bmp'];
    %imwrite(ImageT2,parula,filename1);

    %Image in .tiff format 16bit
    IM16 = uint16(ImageT2);
    filename = ['ImageT2w_MS001_b_slice', num2str(k), '_','.
       tiff'];
    imwrite(IM16,parula,filename);
end
toc
image(ImageT2);
prompt = 'Plot fit ? (Answer by pixel position [X,Y] or no) :
   ';
pix = input(prompt);

while strcmp(pix,'no')==0
    figure();
    plot(echotimes,ymat(128*(pix(1)-1)+pix(2),:),'*r');
    hold on;
    fplot(c{128*(pix(1)-1)+pix(2)},[0,600]);
    prompt = 'Plot fit ? (Answer by pixelnumber or no) :';
    pix = input(prompt);
end
```

MATLAB script for T2* mapping

```
% Original script from matt birkbeck (2022). Parametric
    Mapping Scripts for MRI data (https://www.mathworks.com/
    matlabcentral/fileexchange/64579-parametric-mapping-
    scripts-for-mri-data), MATLAB Central File Exchange.
    Retrieved November 9, 2022.
clear all
clc

tic

%% Loading the data

dname = uigetdir;
dimages = strcat(dname,'/*.IMA');
directory = dir (dimages);
addpath(dname)
files = {directory.name};

%% User selection of the parameters

prompt = 'Number of slices :';
Nbslices = input(prompt);
prompt = 'Number of echoes :';
Nbechoes = input(prompt);
prompt = 'Selection of first echo ? (yes or no) :';
selecfirstecho = input(prompt);
prompt = 'Echo Times :';
echotimes=input(prompt);


%% Creating stacks of slices with their echoes times without
    the first echo

Slices=cell(1,Nbslices);
if strcmp(selecfirstecho,'no') == 1
```

```
    Nbechoes=Nbechoes-1;
else
    Nbechoes=Nbechoes;
end

echo=cell(1,Nbechoes);

if strcmp(selecfirstecho,'no') == 1
    start=Nbslices+1; %Not taking into account the first echo
        for the slices to suppress the first echo
else
    start=1;
end

for k=1:Nbslices
    for j=1:(Nbechoes)
        echo(j)=files(start);
        if start+Nbslices < length(files)
            start=start+Nbslices;
        end
    end
    Slices{k}=echo;
    if start < length(files)
        if strcmp(selecfirstecho,'no') == 1
            start=(start-((Nbechoes)*(Nbslices)))+Nbslices+1;
                %Not taking into account the first echo for
                the slices to suppress the first echo
        else
            start=(start-((Nbechoes)*(Nbslices)))+Nbslices+1;
        end

    end
end
```

```
%% Read dicom files and concatenate them into a (M x N x
   nEchoes x nSlices) Matrix called te_image

Image1 = dicomread(files{1});
[x,y] = size(Image1(:,:,1));
te_image = zeros(x,y,(Nbechoes),Nbslices);

for i=1:length(Slices)
    S=Slices{i};
    for n=1:length(S)
        imecho=S{n};
        te_image(:,:,n,i) = dicomread(imecho);
    end
end

%% Analysis of slices
prompt = 'Slice selection ([first_slice , last_slice]) :';
sliceselec = input(prompt);
C=cell(1,sliceselec(2));

for k = sliceselec(1):sliceselec(2)%size(te_image(:,:,:,:),4)

    Img = te_image(:,:,:,k);
    [x,y,nEcho] = size(Img); % dimension of the Image
    ImageT2=zeros(x,y);
    C{k}=cell(1,x*y);
    c=C{k};

    % to get a 1D array representing our Img matrix the Img
       matrix is
    % re-written to a 1D vector Ydata - this represents our (
       x*y)
    % seperate problems with nEchos data points (nEchos) in
       each problem.
    ymat = reshape(Img,[],nEcho);
```

```
    Xdata=echotimes';

    %fun = @(x,xdata) x(1)*(exp(-xdata/x(2)));

    for i=1:x*y
        if sum(ymat(i,:))~=0
            Ydata=ymat(i,:)';
            %f=lsqcurvefit(fun,[200,90],Xdata,Ydata);
            f=fit(Xdata,Ydata,'exp1');
            if f.b~=0
                T2=-(1/f.b);
                ImageT2(i)=T2;
                h=@(x) (f.a)*(exp(-x/T2));
                c{i}=h;
            end
        end
    end

    %Display the image
    %figure()
    %image(ImageT2);

    %Image in .bmp format
    %filename1 = ['ImageT2w_MC003_004_slice', num2str(k), '_
       ','.bmp'];
    %imwrite(ImageT2,parula,filename1);

    %Image in .tiff format 16bit
    IM16 = uint16(ImageT2);
    filename = ['ImageT2star_MS017_slice', num2str(k), '_','.
       tiff'];
    imwrite(IM16,parula,filename);
end
toc
image(ImageT2);
```

```
126 prompt = 'Plot fit ? (Answer by pixel position [X,Y] or no) :
        ';
127 pix = input(prompt);
128
129 while strcmp(pix,'no')==0
130     figure();
131     plot(echotimes,ymat(128*(pix(1)-1)+pix(2),:),'*r');
132     hold on;
133     fplot(c{128*(pix(1)-1)+pix(2)},[0,600]);
134     prompt = 'Plot fit ? (Answer by pixelnumber or no) :';
135     pix = input(prompt);
136 end
```